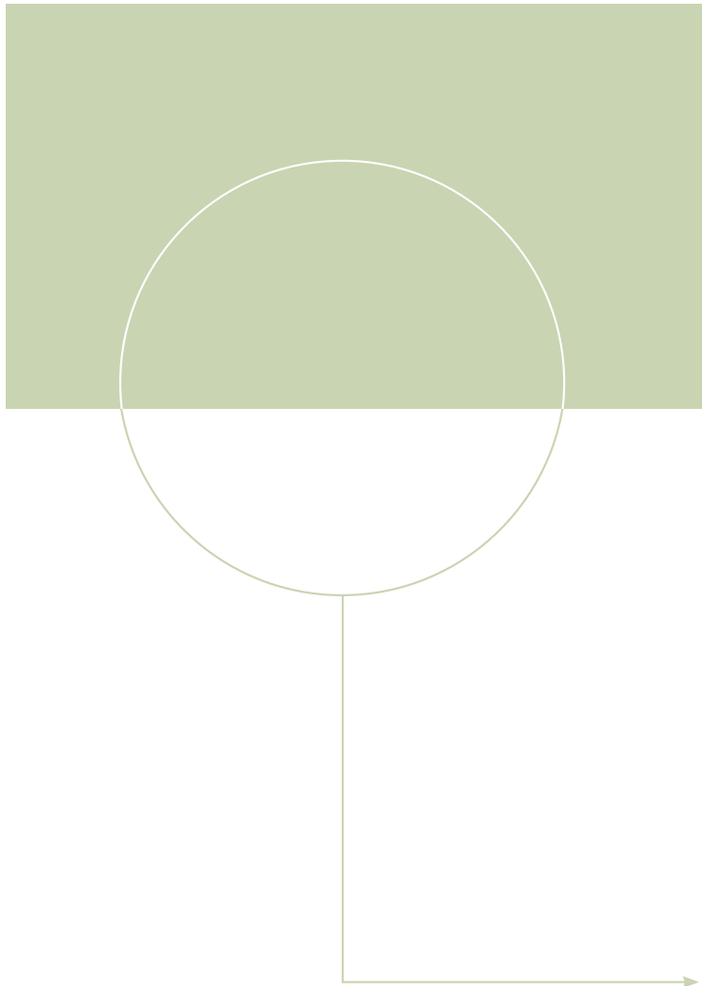

Master's thesis

2020

Ragnhild Fromreide

NTNU
Norwegian University of
Science and Technology
Faculty of Engineering
Department of Civil and Environmental Engineering

Ragnhild Fromreide

Effect of strain-softening behaviour on slope stability during pile driving

June 2020

NTNU
Norwegian University of
Science and Technology

NTNU
Norwegian University of
Science and Technology

NTNU
Norwegian University of
Science and Technology

Effect of strain-softening behaviour on slope stability during pile driving

Ragnhild Fromreide

Civil and Environmental Engineering
Submission date: June 2020
Supervisor: Gudmund Reidar Eiksund
Co-supervisor: Yeganeh Attari

Norwegian University of Science and Technology
Department of Civil and Environmental Engineering

Preface

This Master's thesis in geotechnics at NTNU is the final part of the MSc in Civil and Environmental Engineering. The thesis was carried out during the spring semester of 2020, as a continuation on a specialisation project that was conducted during the fall of 2019. The project is a part of the research project REMEDY, which aims at reducing the risk of damage at the surroundings during construction projects.

The topic of the thesis was suggested by my supervisors Professor Gudmund R. Eiksund and PhD candidate Yeganeh Attari.

Due to the outbreak of the Coronavirus this spring, most of the work with the thesis was conducted in my hometown Sogndal. This gave an unexpected end to my years of studying in Trondheim. Fortunately, the work with the thesis had good progression since I had weekly digital meetings with my supervisors.

The reader of this thesis should be familiar with basic geotechnical theories.

Trondheim, 2020-06-11

Ragnhild Fromreide

Acknowledgement

I would like to thank my supervisors Professor Gudmund R. Eiksund and PhD candidate Yeganeh Attari for their great help and guidance during the work with this thesis. They have always been available for my questions and to discuss problems that I have encountered during this project. A thank you should also be given to Hans Petter Josdal at NGI for the help with the Finite Element modelling.

Lastly, I would like to thank my family, my fellow class mates and my friends for their support during this time.

R.F.

Abstract

The objective of this thesis was to study the effect of strain-softening behaviour during pile driving on slope stability. The work with this thesis aimed at exploring whether a Finite Element model could simulate strain-softening behaviour during pile driving at the crest of a slope. And secondly whether the trigger of strain-softening behaviour could initiate a progressive failure mechanism.

PLAXIS 2D, which is a geotechnical Finite Element program, was used to make a model of pile driving at the crest of a slope. Pile driving was modelled as a volume expansion, simulating the mass displacement that occurs during pile driving. Different constitutive models were tried during the simulations, the Mohr-Coulomb model, the Hardening Soil model and the NGI-ADPsoft model, respectively.

The Mohr-Coulomb model did not manage to capture the destabilising effects of the simulated pile driving. Mainly because of the lack of contractive response during deformations. The Hardening Soil model was modelled with negative dilatancy to account for contractive soil behaviour. A shear stress-strain response that resembled the strain-softening behaviour was obtained, followed by a failure mechanism. The failure mechanism showed tendencies of a progressive failure. However, the strain-softening response seemed to propagate more simultaneously than progressively through the failure surface. Due to the mesh-dependency of the Hardening Soil model with negative dilatancy, these effects were only captured by the model with very fine mesh.

The NGI-ADPsoft model should avoid mesh-dependency by utilising the modified non-local strain approach. The NGI-ADPsoft model was able to simulate a strain-softening response triggered by mass displacements from pile driving. The failure mechanism could to some degree be regarded as progressive. However, it seemed like the approach to replicate pile driving triggered a rigid body movement of the soil, causing a more simultaneous mobilisation of shear strength, than progressively through the failure surface. The simulations with the NGI-ADPsoft model did not overcome the problem of dependent results. To models with different mesh discretisation were run. Only the model with very fine meshing was able to simulate a failure mechanism.

Keywords: Strain-softening, Progressive failure, Pile driving, Slope stability, FEM, NGI-APDsoft

Samandrag

Denne oppgåva tok sikte på å studere effekten av sprø materialoppførsel ved peleramming i nærleiken av ei skråning med sensitiv leire. Føremålet med oppgåva var å utforske om sprø materialoppførsel under peleramming kunne bli modellert i eit elementmetodeprogram. Dernest om initisering av sprø materialoppførsel kunne utløyse ein progressiv brotmekanisme i ei skråning.

Elementmetodeprogrammet PLAXIS 2D blei brukt til å lage ein modell av peleramming på toppen av ei skråning. Pelerammingа blei modellert som ein volumekspansjon av jord, noko som skulle simulere massefortrenginga ved peleramming. Tre materialmodellar vart brukt. Desse var Mohr-Coulomb modellen, Hardening Soil modellen og NGI-ADPsoft modellen.

Mohr-Coulomb modellen klarte ikkje å simulere dei destabiliserande effektane av den modellerte pelerammingа. Hovudsakleg på grunn av at modellen ikkje tok omsyn til kontraktiv materialoppførsel. Hardening Soil modellen vart modellert med negativ dilatans, for å dermed inkludere kontraktiv jordrespons. Ein skjærspenning-tøyningsrepsons som likna responsen ved sprø materialoppførsel vart modellert, med ei påfølgjande brotmekanisme. Brotmekansimen viste tendensar til å vere ein progressiv brotmekanisme. Men den sprø materialoppførselen såg ut til å bre om seg i ein meir samtidig respons enn ein progressiv. På grunn av elementnettavhengnaden som oppstår når Hardening Soil modellen er definert med negativ dilatans, var det kun modellen med fint elementnett som simulerte ein brotmekanisme.

NGI-ADPsoft modellen skal unngå problemet med elementnettavhengnad ved å implementere ikkje-lokal tøyning. Modellen klarte å simulere sprø materialoppførsel utløyst av den modellerte masseforskyvinga, med ein påfølgjande brotmekanisme. Brotmekanismen hadde slik som Hardening Soil modellen, tendensar til progressivt brot. Det såg derimot ut til at måten pelerammingа vart modellert førte til at jorda oppførte seg meir som ein stiv lekam, som førte til ein meir samtidig mobilisering av skjærstyrke gjennom brotflata enn progressivt.

Simuleringane i NGI-ADPsoft modellen omgjekk ikkje problemet med avhengig resultat. To modellar med ulik med elementnettstorleik vart utprøvd. Kun modellen med veldig fint elementnett klarte å simulere ein brotmekanisme.

Contents

List of Figures

List of Tables

List of symbols

Greek symbols

ϕ	Friction angle
ψ	Dilatancy angle
τ	Shear stress
τ_0	Initial shear stress
τ_c	Shear strength along critical failure surface
τ_p	Peak shear stress
τ_r	Post peak shear stress
τ_{mob}	Mobilised shear stress
σ_{max}	Maximal principal stress
σ_{min}	Minimum principal stress
σ_1	Maximal principal stress
σ_3	Minimum principal stress
ϵ_1	Maximal principal strain
γ	Soil density
γ_s	Shear strain
γ_p	Plastic shear strain
γ_p^C	Shear strain at peak undrained triaxial compression strength
γ_p^{DSS}	Shear strain at peak undrained DSS shear strength
γ_p^E	Shear strain at peak undrained triaxial extension strength
$\gamma_p^C{}_r$	Shear strain at residual undrained triaxial compression strength
$\gamma_p^{DSS}{}_r$	Shear strain at residual undrained DSS strength
$\gamma_p^E{}_r$	Shear strain at residual undrained triaxial extension strength
ν'	Drained Poisson's ratio
ν_u	Undrained Poisson's ratio
α	Parameter for "non-local strain"
κ_1	Hardening parameter
κ_2	Softening parameter

Latin symbols

e_{init}	Initial void ratio
e_{max}	Maximal void ratio
p'_c	Effective pre-consolidation stress
p'_0	Initial effective stress
s_u	Undrained shear strength
$s_{u,remould}$	Undrained remoulded shear strength
s_u^a	Undrained active peak shear strength
$s_u^A r$	Undrained active residual shear strength
s_{ur}	Undrained residual shear strength
s_u^P	Undrained passive peak shear strength
$s_u^P r$	Undrained passive residual shear strength
s_u^{DSS}	Undrained DSS peak shear strength
$S_u^{DSS}{}_r$	Undrained DSS residual shear strength
u_0	Initial pore pressure
S_t	Sensitivity
F_s	Factor of safety
Δu	Excess pore pressure
Δu_{max}	Maximal excess pore pressure one day after end of pile driving
$\Delta u / u_0$	Relative excess pore pressure ratio
$\Delta u_{max} / u_0$	Maximal relative excess pore pressure ratio
t_{sb}	Shear band thickness
c'_{ref}	Effective cohesion
E'	Effective stiffness
E_{50}^{ref}	Secant stiffness in drained triaxial test
E_{oed}^{ref}	Tangent stiffness for primary odeometer loading
E_{ur}^{ref}	Unloading/reloading stiffness
m	Power for stress-level dependency of stiffness
k_0	Lateral earth pressure coefficient at rest
G_{ur}	Elastic shear modulus
c_1	Softening parameter 1
c_2	Softening parameter 2
l_{int}	Internal length
k_x	Horizontal permeability
k_y	Vertical permeability

Acronyms

NPRA	The Norwegian Public Roads Administration
CAUc	Anisotropic consolidation undrained compression
CAUe	Anisotropic consolidation undrained extension
DSS	Direct simple shear
FOS	Factor of safety
FEA	Finite element analysis
FEM	Finite element method
HS	Hardening Soil
MC	Mohr-Coulomb
NC	Normally consolidated
NGI	Norwegian Geotechnical Institute
NVE	Norges Vassdrags- og Energidirektorat (The Norwegian Water Resources and Energy Directorate)
3D	Three-dimensional
2D	Two-dimensional

Chapter 1

Introduction

Stability of slopes is an important matter specifically in areas with high volumes of loose sands or soft clay. In Scandinavia it is more of a sensitive issue considering the existence of quick clay areas (Rosenqvist, 1953). Soft and sensitive clays such as quick clays have a tendency of showing brittle soil behaviour when subjected to rapid loadings that trigger the undrained behaviour of the soil. These soil types may experience a significant loss of shearing resistance during undrained loading, referred to as strain-softening behaviour (Bjerrum, 1968).

Pile driving is often necessary to conduct near a slope, especially when building foundations for bridges. The disturbances from pile driving, in terms of mass displacements, vibrations of the soil and loads from the machines, may have destabilising effect on a slope and in worst case lead to slope failure. A failure mechanism induced by pile driving may start with a small region of the soil getting overstressed and by that experience strain-softening behaviour. Continued disturbances from pile driving, may cause a gradual progression of strain-softening behaviour throughout the slope. This can ultimately result in the global failure of the slope in a progressive failure manner (Grivas and Chowdhury, 1982).

Geotechnical engineers often have to assess stability of the slope during pile driving. Limit Equilibrium Methods (LEM) are the conventional and most common methods of assessing slope stability problems during pile driving. However, there are several examples of conducted stability analyses that insured sufficient stability during and in short time after the conducted pile driving, and still slope failure occurred (Bernander, 1978). A challenge with the LEM is that it fails to capture the strain-softening behaviour of brittle soils (Bernander, 1978). An alternative to as-

sess slope stability by means of LEM, is therefore to use numerical methods such as the Finite Element Method (FEM).

1.1 Initial research

The work with this thesis started with a study which aimed at studying the effect of pile driving on slope stability. A case study was conducted on a construction project in Fredrikstad during the building of a bridge called "Klaffebru". Slope failure occurred during pile driving for one of the foundations of the bridge. A short summary of the initial work from this project report (Fromreide, 2019) is given below.

From the study on effects of pile driving on slope stability, mass displacements during pile installation was proved to be one of the main disturbances. The effect of mass displacement on slope stability was studied by means of numerical analyses using the geotechnical finite element program PLAXIS 2D.

The main challenge was to study how may mass displacement initiate failure in a slope. The effect of the simulated pile driving was studied in an elasto-plastic Mohr-Coulomb model. This was carried out by laterally expanding 0.5 m wide clusters of soil at the crest of the slope. The primary focus was on studying how excess pore pressure generation due to pile driving may affect slope stability. However, such simulations, specifically in a total stress state, proved to have little effect on slope stability and did not initiate failure. The reason was that an increase of pore pressure in an undrained elasto-plastic total stress model does not affect the effective stress situation and as a result soil strength remains unchanged. With no change in the soil strength, such simulations do not provide a reduction in the factor of safety of the slope during pile driving and cannot represent any failure mechanism.

It was thus deemed necessary to have a change of focus. The focus was then shifted to whether it was possible that strain-softening behaviour and progressive failure could trigger slope failure during pile driving. New research questions were formed for the continuation of work with this Master's thesis. For this part of the study, an arbitrary slope geometry was chosen for an easier understanding of failure mechanism and affecting parameters.

1.2 Problem formulation

This thesis aims at studying how strain-softening behaviour may be initiated during pile driving in soft and sensitive clay soil. Further how the initiation of strain-softening behaviour may trigger progressive failure when pile driving is conducted near a slope. The work with this thesis will try to answer the following research questions:

- Can finite element methods simulate the strain-softening of the soil material during pile driving?
- Can a simulation of pile driving in a finite element program initiate a progressive failure mechanism?

1.3 Limitations

The focus of this thesis is at the effect of mass displacements during pile driving. There are however other effects that creates disturbances during pile driving which is not accounted for in these simulations. These are for instance vibrations of the soil induced during pile driving and loads from the machines conducting the pile driving.

Pile driving affects the surrounding soil in a three-dimensional (3D) space. The simulations are however conducted in the two-dimensional (2D) version of the program PLAXIS. Information gets lost in the process of implementing a 3D problem into a 2D space.

1.4 Structure of the thesis

The thesis is divided into 7 chapters:

Chapter 1: Introduction of the topic, a summary of the start of the project and a presentation of the problem formulation.

Chapter 2: Presents the geotechnical background knowledge for the problem.

Chapter 3: Contains some of the fundamental theory around strain-softening and progressive failure.

Chapter 4: The constitutive models are presented and a description of the finite element modelling approach in PLAXIS 2D.

Chapter 5: Presents the results from the analyses in PLAXIS.

Chapter 6: Discussion of the results.

Chapter 7: Conclusion and recommendations for further work.

Chapter 2

Background

2.1 Soft and sensitive clay

The behaviour of soft and sensitive clay is an especially relevant topic in Scandinavia, due to large deposits of quick clays (Rosenqvist, 1953). Sensitive clays are often described in terms of the sensitivity. The sensitivity is defined as the ratio between the undisturbed shear strength, s_u, and the remoulded shear strength, $s_{u,remould}$ (Eurocode 7, 2007):

$$S_t = \frac{s_u}{s_{u,remould}} \tag{2.1}$$

The Norwegian Public Roads Administration (NPRA) classifies sensitive clay as shown in table 2.1.

Table 2.1: Classification of sensitivity of clay (Statens Vegvesen, 2005).

Clay	Sensitivity
Low sensitivity	< 8
Medium sensitive	8-30
Very sensitive	> 30

A soft clay can be classified by the means of its undrained shear strength, as done by the NPRA in table 2.2.

Table 2.2: Classification of clay (Statens Vegvesen, 2005).

Clay	Shear strength [kPa]
Soft	<25
Medium	25-50
Firm	>50

The Norwegian Water Resources and Energy Directorate (NVE) classify a clay that has a remoulded shear strength $s_{u,remould} < 2$ kPa and a sensitivity $S_t > 15$, as a clay that holds the properties of showing brittle soil behaviour (NVE, 2014).

2.2 Effect of pile driving in clay soil

Piles are used as a foundation method to transfer loads from buildings and bridges to deep layers of soil or down to bedrock. Piles are mainly installed by either pile driving or installation in a pre-bored hole. This thesis focuses at the disturbing effects from pile driving.

Pile driving can induce severe disturbances to the surrounding soil. During the installation, a soil volume equal to the volume of the piles have to be displaced in order to make room for the driven piles (Flaate, 1971). The displaced soil is forced in both vertical and horizontal direction, depending on the direction of least resistance (Flaate, 1971). Due to the induced mass displacement, a plastic radius develops around the pile where the soil is highly remoulded (Langford and Sandene, 2015), shown in figure 2.1. The effect reduces with distance from the driven pile. It is however challenging to predict these disturbing effects when the piles a driven in groups (Langford and Sandene, 2015). The magnitude of such disturbances depends on several factors such as the number of piles being driven, type of piles, rate of piling and the properties of the soil the piles are being driven into (Flaate, 1971).

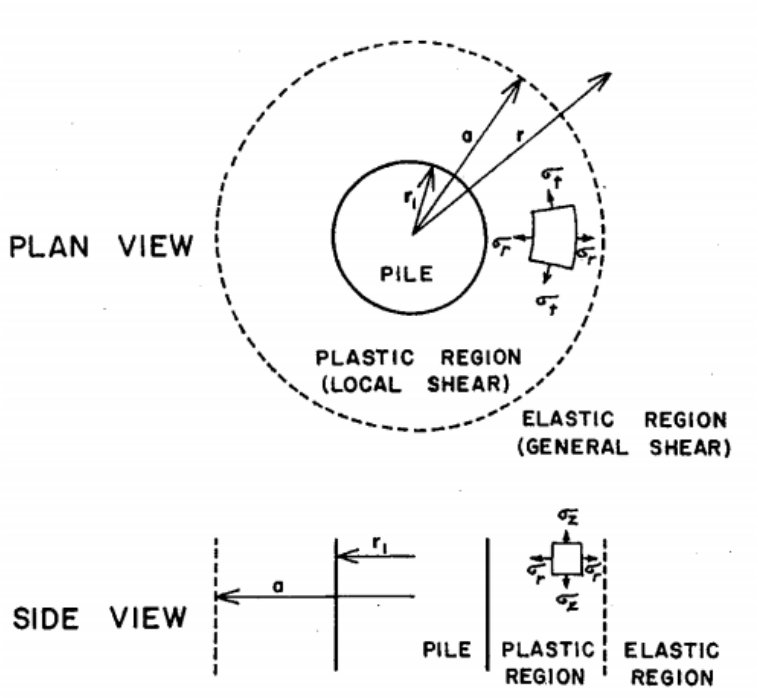

Figure 2.1: The visualisation of the plastic region occurring around a driven pile, from Airhart et al. (1967).

The mass displacement and the remoulding of the soil cause in turn a rapid increase of excess pore pressure (Bjerrum and Johannessen, 1961). Due to the low permeability of clays, the rapid disturbance from the pile installation triggers an undrained behaviour of the soil (Duncan et al., 2014). The increase in pore pressure originates from two effects, an increase of total mean stress and shearing of the soil (Massarsch and Broms, 1981; Thakur et al., 2005).

A change in the total mean stress situation does not affect the shear strength of the soil. Since the increase in total mean stress only comes from increase of pore pressure, and consequently does not affect the effective stress situation (Duncan et al., 2014).

However, the shear-induced pore pressure does in contrary affect the shear strength of the soil. Shear-induced pore pressure originates from the soil either dilating or contracting during shear deformations. A soft and sensitive soil will normally contract when subjected to shear deformations (Thakur et al., 2005). Which means that the soil volume compresses and generates excess pore pressure (Duncan et al., 2014). As a result of the generated excess pore pressure, the effective stresses decreases and consequently the soil experience reduced shear strength (Duncan et al., 2014).

Due to the disturbing effects from pile driving in clays, there is a risk of slope failure (Bernander, 1978). It is therefore important to conduct a slope stability analyses to ensure sufficient safety during pile installations.

2.3 Current practice of slope stability analyses during pile driving in slopes

The conventional methods of assessing slope stability problems are by Limit Equilibrium Methods (LEM). LEM finds the critical failure surface by finding the surface giving the minimum Factor of Safety, F_s. The Factor of Safety is defined as the ratio between the shear strength along the critical failure surface, τ_c and the current shear stress along this surface, τ (Janbu, 1973), given by the following equation:

$$F_s = \frac{\tau_c}{\tau}. \tag{2.2}$$

The factor of safety says something about how much shear strength is available before the slope reaches failure. When the shear stress is equal to $\tau = \tau_c / F_s$, the slope has reached a state of limit equilibrium (Janbu, 1973). If the factor of safety becomes less than one, $F < 1$, the slope is no longer stable, and failure occurs.

There is currently no general method on how to assess slope stability during pile driving (Langford and Sandene, 2015). However, one method that is used in several projects is to estimate the increase of excess pore pressure due to pile driving based on empirical methods, and further decrease the undrained shear strength accordingly or apply the pore pressure profiles into a limit equilibrium analysis (Langford and Sandene, 2015). The Klaffebru project in Fredrikstad and the Øvre Sund bridge in Drammen are examples of projects where this method was used to evaluate the slope stability during pile driving (Johansen and Finstad, 2009; Fredriksen, 2013).

The magnitude of excess pore pressure for the projects was determined by the method suggested by Hoem (1975). Hoem (1975) collected pore pressure measurements due to pile driving from seven different construction projects. Figure 2.2 shows a relationship between the maximal relative excess pore pressure ratio, $\Delta u_{max} / u_0$ and mass displacements, $(d/l)^2$ due to the driven piles one day after the piling had finished.

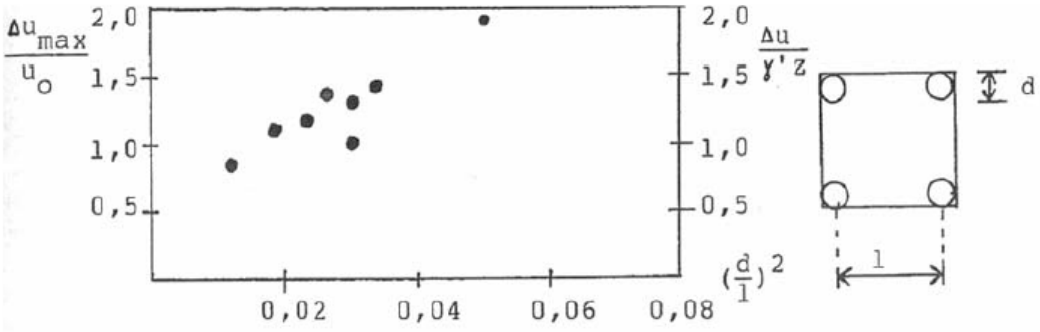

Figure 2.2: Relative excess pore pressure ratio with mass displacement induced by pile driving (based on Hoem (1975) and further adjusted by Berg-Knutsen (1986))

The trend observed in figure 2.3 may be described by the following equation:

$$\Delta u_{max} = (30 \cdot (d/L)^2 + 0.5) \cdot p_0', \tag{2.3}$$

where Δu_{max} is the maximal excess pore pressure one day after the end of pile driving, d is the pile diameter, L is the centre to centre distance between the piles and p_0' is the initial effective stress (Hoem, 1975). The excess pore pressure was determined at different distances, R, from the pile group with the use of the graph in figure 2.3.

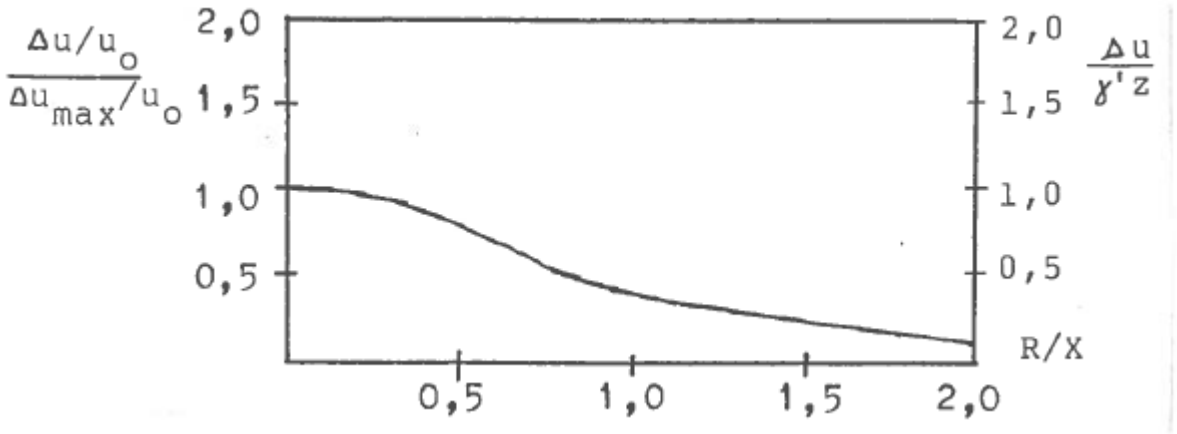

Figure 2.3: Excess pore pressure ratio with distance from the centre of pile group. R is the distance from the centre of the pile group, X is the width of the pile group and $\Delta u/u_0$ is the relative excess pore pressure ratio (based on Hoem (1975) and further adjusted by Berg-Knutsen (1986))

The shear strength of the soil was reduced based on the estimated pore pressure increase. Sta-

bility calculations could then be conducted to assess the short-term stability during the pile installation. Based on the stability analyses, limits of how high the pore pressure could rise and still ensure slope stability during pile driving were established. Measurement of pore pressure were conducted on site to ensure that the pore pressure levels did not exceed these limits. (Johansen and Finstad, 2009; Fredriksen, 2013)

2.4 Challenges with the current approach

In contrary to finite element methods, limit equilibrium analysis neglects the stress-strain behaviour of the soil (Prévost and Höeg, 1975). LEM assumes the soil material to behave as a rigid body considering that it follows the perfectly plastic Mohr-Coulomb failure criterion at failure (Prévost and Höeg, 1975; Yu et al., 1998). This method assumes a peak shear strength along the entire slip surface regardless of the extent of strain development (Bonadies et al., 2014). This can lead to inaccurate results specifically when analysing slopes in quick clay areas or in soft sensitive clays where reduced shear strength might be representative value along the shear surface, hence, failing to predict progressive failure (Jostad et al., 2014; Bonadies et al., 2014). The development of stresses at the failure surface are strain dependent, which cannot be captured by LEM. This mechanism can only be described by the means of numerical methods, such as the Finite Element Method (Andresen and Jostad, 2007).

Figure 2.4 shows the difference of shear stress-strain behaviour between a perfectly plastic material and a sensitive brittle clay, as curve A and curve C respectively.

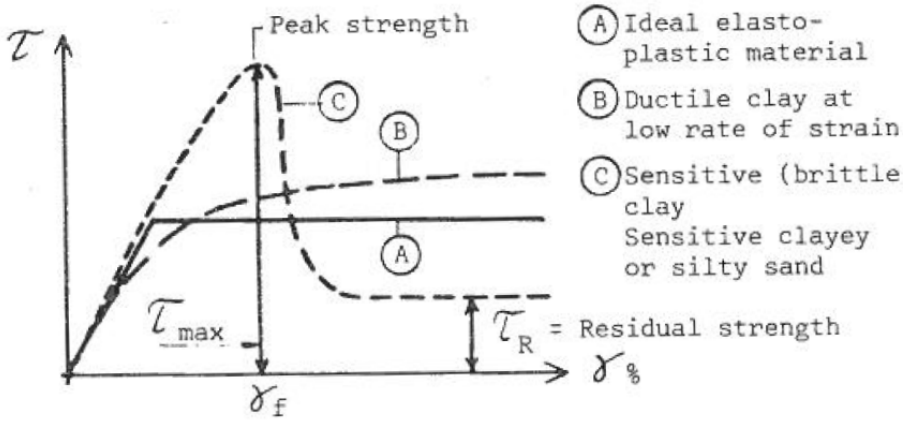

Figure 2.4: Illustration of the shear stress-strain behaviour for different types of soil, from Bernander (1978).

The approach of assessing slope stability during pile driving, explained in the previous section, assumes that the generated excess pore pressure reduces the effective stresses in the soil and consequently that the shear strength reduces. However, the increased excess pore pressure that stems from an increase in total mean stress will not affect the effective stresses in short-time for cohesive soil. To base the decrease in shear strength from pore pressure measurements that comes from both a change in total stress and from shearing of the soil structure will hence misleading. Thus it is only shear-induced pore pressure from the contractive soil response that may reduce effective stresses in the soil and ultimately reduce shear strength.

2.5 Failures induced by pile driving

There are several examples where safety analyses of pile driving in slopes with the use of conventional methods of limit equilibrium and perfectly plastic soil behaviour showed sufficient capacity against failure, nevertheless slope failure occurred. A few examples of such failures are mentioned below.

A pile installation project in Rävekärr, Sweden in 1971 caused a 550 m long crack to appear. A similar incident happened at a piling project in Björnlandavägen in Sweden, where the pile driving initiated a 200 m long crack. Both failures were regarded as unfinished landslides since the slope inclination was not steep enough for global slope failure to occur (Bernander, 1978). The conducted slope stability analyses in advance of the pile driving showed sufficient capacity against failure, and still this soil failure initiated (Bernander, 1978). A landslide at Rollsbo in Sweden was triggered by driving of sand drains. The safety analysis beforehand gave a factor of safety to 2.3, which is considered as relatively high safety against failure. Bernander (1978) stated that the only explanation of the failures at Rävekärr, Björnlandavägen and Rollsbo could be due to brittle, progressive failures.

A slope failure in Surte, Sweden in 1950 turned into a massive landslide, inflicting excessive damages to the surroundings. The failure was triggered by pile driving for the construction of a family house. A progressive failure mechanism was likely induced by a local rise of excess pore pressure which led to a loss of shearing resistance in small coarse layers in the clay stratum (Bernander et al., 2016). The landslide is an example of how a local disturbance may trigger massive destructions.

A slope failure due to dredging and pile driving occurred at an underwater slope in Portland, Maine, in the US. The conducted safety analyses in advance resulted in a factor of safety greater than 1.5, which was calculated based on the peak shear strength. However, the soil testing revealed strain-softening behaviour of the soil. Soil disturbances due to dredging and following pile driving likely caused a drop of shearing resistance in the failure zone and failure then initiated. (LaGatta and Whiteside, 1984)

These examples show that calculated safety from conventional methods of analysis cannot always ensure stability. Pile driving may induce brittle failures despite conventional analyses suggesting sufficient safety against failure (Bernander, 1978). Bernander (1978) stated that including analyses of brittle progressive failures and by considering limited plasticity of soils in geotechnical design would, reduce the risk of soil failures.

Chapter 3

Theory

3.1 Strain-softening behaviour

As previously mentioned, soft and sensitive clay has a tendency of showing brittle soil behaviour when subjected to shear deformations, also known as strain-softening behaviour (Bernander, 1978). A brittle soil subjected to shear strains will first reach its peak shear strength, and continued plastic straining cause the soil to experience a significant loss of shearing resistance. (Bjerrum, 1968; Prévost and Höeg, 1975; Grivas and Chowdhury, 1982). The soil ultimately reaches a state of constant residual shear strength (Bjerrum, 1968). Figure 3.1 shows an illustration by Thakur et al. (2014) of the response of a soft and sensitive clay when subjected to undrained shearing. Soft and sensitive clay tends to show contractive behaviour during shear loading. After reaching a peak shear stress, τ_p, follows a phase of post-peak softening, where the shear stresses reduce due to the diminishing of effective stresses from a generation of shear-induced pore pressure. Eventually, the soil reaches a state of constant shear stress, attaining the post peak shear stress, τ_r. (Thakur et al., 2014)

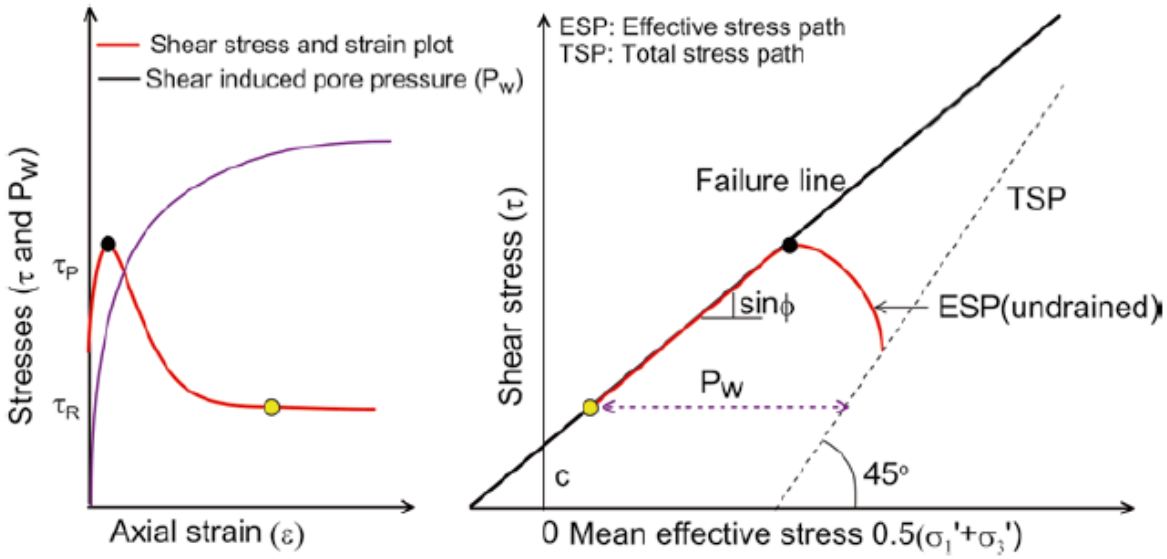

Figure 3.1: An idealised representation of undrained strain-softening due to shear-induced pore pressure generation of soft and sensitive clay up to 20% straining level, from Thakur et al. (2014).

There are different ways to explain strain-softening behaviour. Skempton (1964) was one of the first to try to explain strain-softening behaviour of soils. He related the reduction in shear strength during high level shearing to a decrease in both the cohesion and friction angle. Bjerrum (1961), on the other hand, explained the reduction in shear strength due the development of shear induced excess pore pressure. The latest research seems to relate strain-softening behaviour due to development of shear induced pore pressure (e.g. Gylland et al. (2014); Thakur et al. (2014); Thakur (2007)).

Thakur et al. (2014) conducted a study on six different clays with soft and sensitive properties by preforming CAUc triaxial tests. The test showed clear indications that strain-softening on soft sensitive clays during undrained conditions exposed to $10-20\%$ straining came from shear-induced pore pressure. According to Thakur et al. (2014), cohesion and friction softening at soft sensitive clay could on the other hand occur at very high strain levels.

The brittleness of the soil can be described by the brittleness ratio, s_{ur}/s_u, where s_{ur} is the undrained residual shear strength and s_u is the undrained peak shear strength (Bernander and Svensk, 1982). The lower the brittleness ratio, the higher the loss of shearing resistance becomes. According to Bernander and Svensk (1982), the brittleness ratio may become as low as 0.3 for soft clays at strain rates similar of those occurring at an actual landslide. To which extent the

shear stresses reduces from the peak stress depends on several properties, such as the OCR, the drainage conditions and how generation of excess pore pressure affect the clay structure (Grivas and Chowdhury, 1982).

The stress-strain response for a brittle clay seem to be dependent of strain rates during testing. Gylland (2012) conducted triaxial tests with different strain rates on a Norwegian quick clay. The obtained stress-displacement curves in figure 3.2 clearly shows that an increased rate of straining led to a higher peak shear strength and a more rapid decrease of shear resistance in the post-peak state.

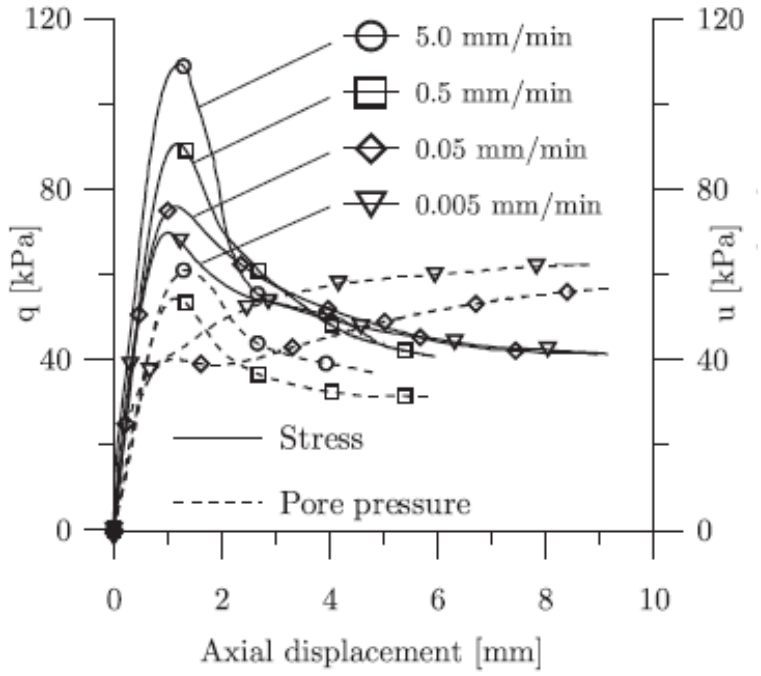

Figure 3.2: Stress-displacement curves from triaxial tests with different rates of straining, from Gylland (2012).

3.2 Progressive failure

Once one part of the soil experiences local failure due to strain-softening, there is a tendency of propagation of the failure within the soil body. The softening process may be initiated by limited zones getting over-stressed. Firstly, the soil reaches its undrained peak strength due to increased level of strains. As the plastic straining continues, the shear strength decreases towards its residual strength and local failure occurs. Because of this strength reduction, the loads

have to be redistributed to the adjacent soil. The redistribution of loads leads to the possibility that these parts may also become over-stressed and hence, reach failure. Once again, the loads get redistributed and other regions experience the same softening. In this way, the failure region propagates progressively through the soil. A phenomenon that is called progressive failure (Grivas and Chowdhury, 1982). The illustration by Andresen and Jostad (2007) in figure 3.3 shows how a failure region may progress within a slope and induce global failure. Failure occurs first at the toe of the slope and progresses backwards towards the crest as the soil experiences excessive straining.

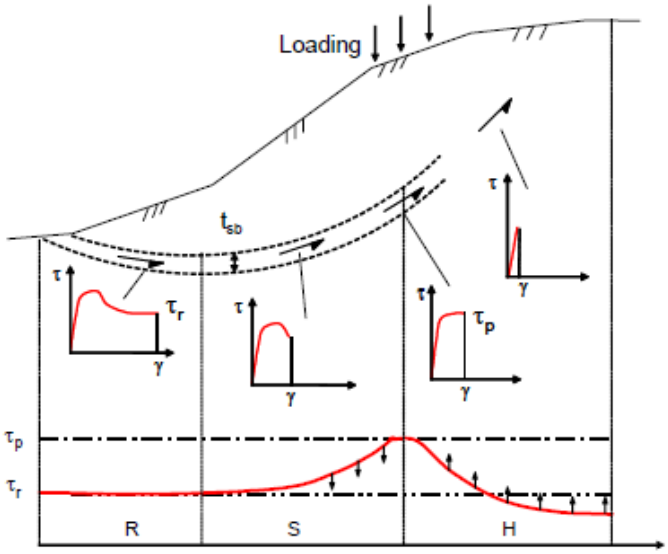

Figure 3.3: The figure illustrates the progression of strain-softening behaviour leading to a rotational progressive failure mechanism, from Andresen and Jostad (2007)

Progressive failure in slopes may be triggered by a disturbance at the crest of a slope (Locat et al., 2011). Pile driving is an example of such a disturbance, and it can be illustrated as the loading shown in figure 3.3. The disturbance may cause an increased mobilisation of shear stresses in the soil, leading to strain-softening behaviour. The consequence of strain-softening propagating in the soil mass can be that soil cannot withstand the disturbances from the ongoing pile driving (Locat et al., 2011). Hence, progressive failure gets triggered and it may initiate a global failure of the slope.

3.3 Shear band localisation

Soils with strain-softening properties are often characterised as unstable materials (Gylland et al., 2014). Due to the instability, the formation of shear bands within the soil may occur when the soil is subjected to shear strains. These shear bands, or strain localisations, are small regions where plastic strains initiate and accumulate (Gylland et al., 2014). The deformations within the shear bands are not unique (Jostad et al., 2014), which makes the strain propagation hard to predict.

The illustration by Andresen and Jostad (2007) in figure 3.4 shows the occurrence of a shear band in a direct simple shear (DSS) test. The development of a shear band leads to a non-uniform distribution of the developed strains coming from the prescribed horizontal displacement in the DSS test (Jostad et al., 2014). A non-uniform distribution of strains in the soil element means that the plastic strains accumulate inside the shear band, and the soil outside this zone experiences elastic unloading in terms of stress relief and decreased shear strains (Jostad et al., 2014; Gylland et al., 2014; Thakur, 2011). The shear band thickness, t_{sb}, controls the degree of softening and therefore also how much disturbance the soil can withstand before reaching failure (Jostad and Andresen, 2002). The degree of softening means how steep the softening curve becomes in shear stress-shear strain curve after the peak strength is reached (Jostad et al., 2006).

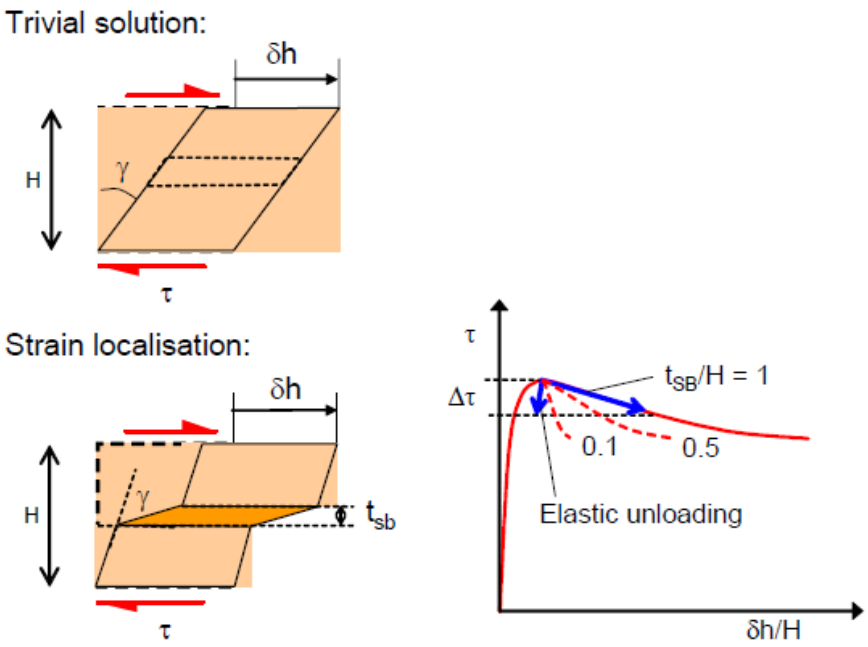

Figure 3.4: Direct simple shear test on a sample, showing the difference between a uniform trivial solution and a strain localisation in a shear band, from Andresen and Jostad (2007).

Inside the shear bands, excess pore pressure develops, occurring especially for sensitive clays. Whereas the soil outside ideally experience no pore pressure development (Gylland et al., 2014; Thakur, 2007). A non-uniform pore pressure situation occurs for globally undrained boundary conditions (Gylland et al., 2014). However, some excess pore pressure will often generate at the elastic unloading part of the soil as well, originating from the shear band or due to kinematic compression (Thakur, 2007).

The shear band thickness, t_{sb}, for coarse grained soils are often set equal to the grain size. However, it is not as easily determined for fine grained soils (Andresen and Jostad, 2007). Multiple studies on soft sensitive clay show that the shear band thickness is very dependent on rate of straining (Gylland et al., 2014; Jostad et al., 2006; Thakur, 2011). And that increased rate of straining results in decreased shear band thickness (Jostad et al., 2006; Gylland et al., 2014). According to research by Thakur (2007), the shear band thickness in soft and sensitive clay at the onset of strain localisation measured between 3 and 4 mm.

Chapter 4

Finite element modelling

The mechanism of strain-softening behaviour and progressive failure have to be analysed by means of numerical methods such as finite element modelling (Andresen and Jostad, 2004). The Finite Element Method is a numerical analysis that gives an approximate solution to a structural problem (Huebner et al., 2001), which for this case was a slope stability problem. FEM discretise the slope into small finite elements creating a mesh, and by that reducing the problem into smaller parts (Huebner et al., 2001). Constitutive models describe the soil behaviour by a set mathematical equations relating the stress-strain relationship of the soil to material points at the inside and at the boarder of the elements (Lade, 2005). The quality of the solution is thus dependent on the number of elements and material points as well as the choice of constitutive models (Huebner et al., 2001; Lade, 2005). The geotechnical finite element program PLAXIS 2D provides several constitutive models that in different ways describe the soil behaviour and establishes a failure criterion with varying degrees of complexity.

FEM ensure equilibrium of the soil by distributing the stresses between the elements of the slope. If an element experience stresses that surpass the failure criterion of the model, the stresses gets redistributed to the neighbouring elements to maintain equilibrium. If such a redistribution is not able to reduce the stresses beneath the acceptable limit in that area, failure initiates (Griffiths and Lane, 1999). A propagation of a failure surface develops as more of the soil exceed the yield limit. Global failure occurs when a sufficient amount of material points has yielded and a failure surface has developed (Griffiths and Lane, 1999). In contrast to LEM, it is not necessary in a FE analysis to make an assumption in advance regarding the shape and loca-

tion of the critical failure surface (Griffiths and Lane, 1999). The FEM finds the critical surface whilst analysing the problem at hand.

When a slope has reached its critical state and instability has occurred at an area in the soil, a soil exhibiting strain-softening behaviour has reached different stages at the shear-stress strain curve (Jostad and Andresen, 2002). This behaviour is illustrated in figure 3.3. There has one part of the slope reached the residual state, one part at the post-peak state, one part at the peak strength, and one part has only reached the elastic part of the soil. There is no critical surface where the peak shear strength is mobilised along the entire surface, as the LEM is based on. The capacity of the slope depends on the complete stress-strain behaviour of the clay, including the non-linear behaviour (Jostad and Andresen, 2002). It is, therefore, necessary to use modelling approaches that account for the non-linear stress-strain relationship of the soil (Jostad and Andresen, 2002).

The strain-softening behaviour induced by pile driving near a slope, was studied by making a model in the geotechnical finite element program PLAXIS 2D. The aim of the practice was to see whether a finite element model could simulate the development of strain-softening behaviour due to pile driving, ultimately leading to a progressive failure. This was done by using three different constitutive models in PLAXIS 2D, the Mohr-Coulomb model, the Hardening Soil model and the NGI-APDsoft model. The models are described in the following section.

4.1 Constitutive soil models

4.1.1 The Mohr-Coulomb model

The Mohr-Coulomb (MC) model is an elastic perfectly plastic soil model in PLAXIS (PLAXIS, 2018). The model treats the deformations of the soil as either elastic or plastic. The soil behaves elastically during deformations as long as the stresses are below the yield surface. If the stresses exceed the yield surface, plastic deformations occur. The yield surface based on the Mohr-Coulomb failure criterion is defined by the input parameters, which means that it is fixed and not affected by plastic straining (PLAXIS, 2018). The yield function is defined as follows:

$$f = (\sigma_{max} - \sigma_{min}) - 2c \cdot \cos\phi - (\sigma_{max} + \sigma_{min}) \sin\phi \tag{4.1}$$

where σ_{max} and σ_{min} is maximum and minimum principal stress, respectively, c is the cohesion and ϕ is the friction angle (PLAXIS, 2018). The yield surfaces are shown in figure 4.1 in a principal stress space.

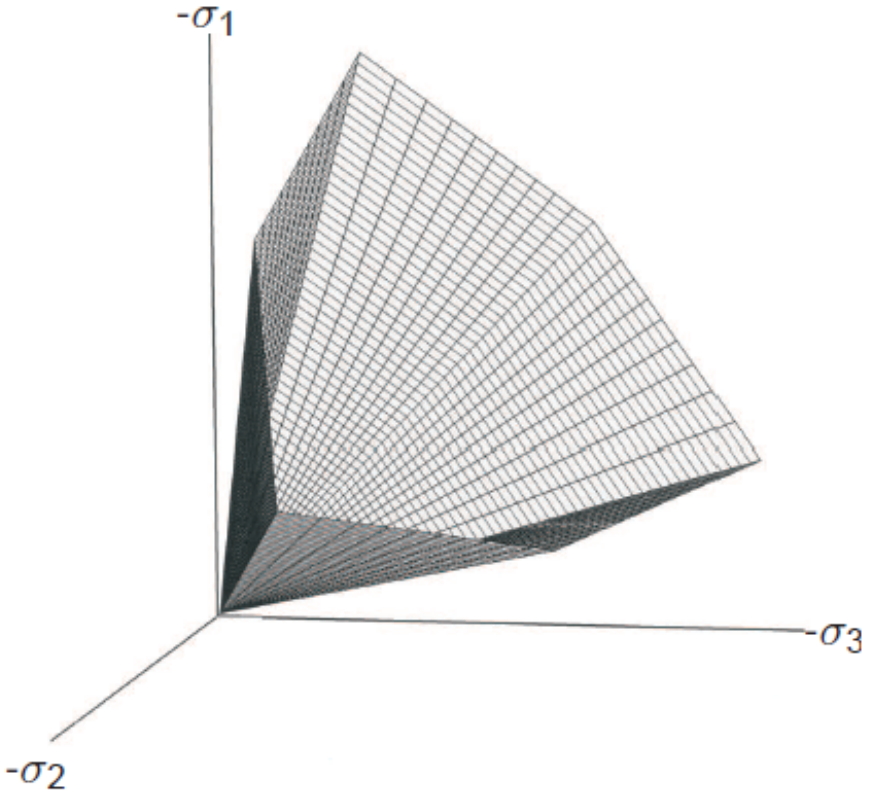

Figure 4.1: The yield surfaces in a principal stress space, (c=0), for the Mohr-Coulomb model, from PLAXIS (2018).

The input parameters are given in section 4.2.2.

4.1.2 The Hardening Soil model

The Hardening Soil (HS) model is an advanced material model in PLAXIS (PLAXIS, 2018). The most important features with this model that differentiate it from other constitutive models are; the model is based on the theory of plasticity, it can model soil dilatancy and it introduces a yielding cap. (Schanz et al., 2000; PLAXIS, 2018).

The model requires three stiffness parameters as input. These are the secant stiffness in a standard drained triaxial test, E_{50}^{ref}, the tangent stiffness for primary odedometer loading, E_{oed}^{ref}, and the unloading/reloading stiffness E_{ur}^{ref} (Schanz et al., 2000). The stiffness in the HS-model depends on the effective stress level, resulting in the stiffness increasing with increasing stress level

(Schanz et al., 2000).

The HS-model does not fix the yield surface in a principle stress state like the elastic perfectly-plastic model does. The yield surface in the HS-model may on the other hand expand when the soil is subjected to plastic strains (Schanz et al., 2000). Figure 4.2 shows the yield surface described by the Mohr-Coulomb criterion. The lines below the MC failure line represent different degrees of mobilisation of the failure criterion. As the soil experience increased plastic straining, the yield surface expands towards the failure line. During an unloading, the yield surface will remain in its outermost position and inside this region, the soil behaves elastically (Nordal, 2019).

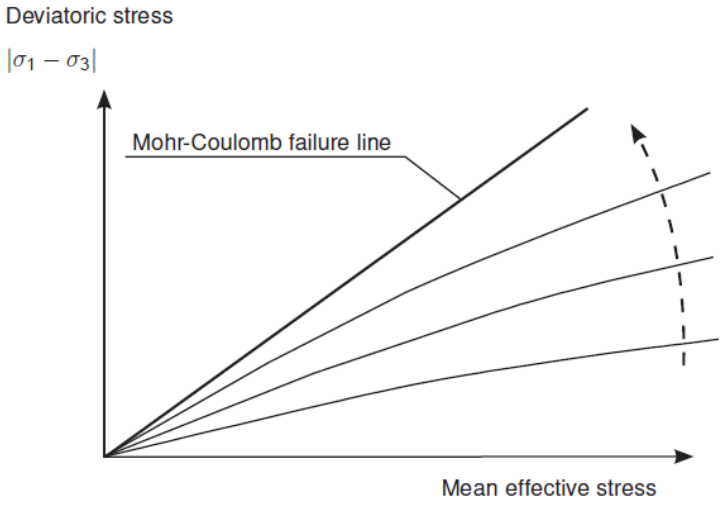

Figure 4.2: An illustration of the yield surface for the HS-model described by the Mohr-Coulomb failure criterion, from PLAXIS (2018).

The yield surface in figure 4.2 limits the plastic shear induced strains of the soil. However, it does not describe the plastic volume strains the soil may experience during isotropic compression (Schanz et al., 2000). The model therefore introduces a second yield surface, referred to as the cap surface, illustrated in figure 4.3. The cap surface encloses the elastic region in the mean stress direction, hence the p-axis. The cap is determined from the pre-consolidation stress, p'_c. If the stress situation in the soil exceeds the p'_c, the cap expands and the soil experience plastic volumetric strains. The E^{ref}_{oed} largely determines the amount of plastic volumetric strains coming from the yielding cap, whereas the E^{ref}_{50} determines the plastic shear strains coming from the shear yield surface. (Schanz et al., 2000)

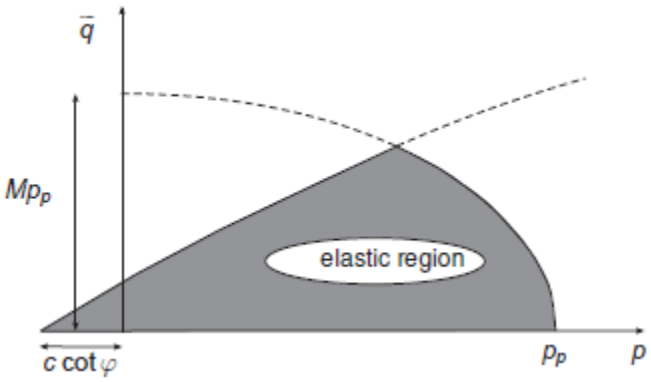

Figure 4.3: An illustration of the yield surfaces in a HS-model in a p-q plot, from (PLAXIS, 2018).

The Hardening Soil model modelling strain-softening behaviour

The purpose of the model was to achieve strain-softening behaviour induced by the simulated pile driving. Most stability problems are modelled by setting the dilatancy angle, ψ, equal or higher than zero. However, by using a negative dilatancy angle, $\psi < 0$, the model will also account for strain-softening and may simulate progressive failure (Thakur et al., 2006).

The problem with the use of a negative dilatancy angle is the occurrence of numerical instability in the model. The results become mesh dependent. This means that the results from the analysis depends on the thickness and orientation of the shear bands, where the mesh size is used as an internal length parameter (D'Ignazio and Länsivaara, 2015). Running the analysis with different mesh sizes gives different results. It therefore makes it hard to use these models in practical engineering. Regardless of this knowledge, the purpose of this model is to see if the modelled pile driving may trigger strain-softening behaviour and lead to failure of the slope. The model will be studied at a theoretical level to provide insight for practical applications and incomplete guidelines.

The propagation of dilatancy in the HS-model can be controlled by using the dilatancy cut-off function. The end of dilatancy occurs when the soil, after being exposed to substantial shearing, reaches its critical state density. This behaviour is controlled by the two parameters, the initial void ratio, e_{init}, and the maximal void ratio, e_{max}. When the soil has reached its maximum void ratio due to shearing, the mobilised dilatancy angle is set to zero. (PLAXIS, 2018)

However, the dilatancy cut-off did not appear to work. As it did not seem to affect the stress-strain behaviour of the soil. The end of dilatancy was therefore modelled by using the tension

cut-off function in PLAXIS. The tension cut-off function lets the user define allowable limits of tensile strength (PLAXIS, 2019). In this case the default value was chosen, which is zero tensile strength (PLAXIS, 2019). Figure 4.4 demonstrates by the use of the soil test function in PLAXIS, the difference in whether or not tension cut-off was activated. Without tension cut-off, the mobilised shear stresses reduced towards zero during deformations. Whereas with tension cut-off activated, the shear stresses reduced towards a limit and then became constant. This resembled strain-softening behaviour and was thus chosen in the model.

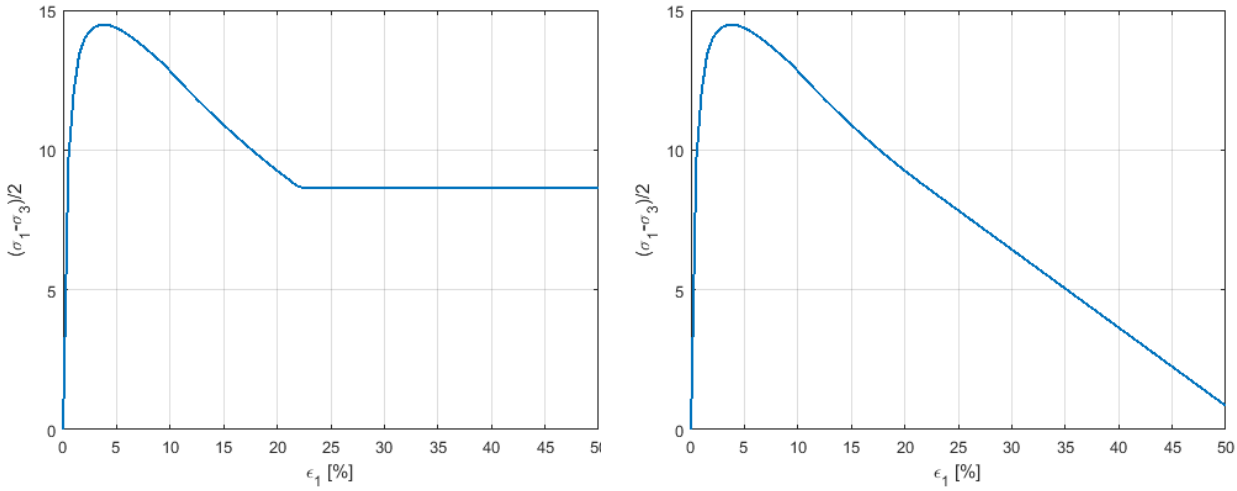

(a) With tension cut-off.

(b) Without tension cut-off.

Figure 4.4: Plots of shear stress-strain curves during soil testing.

4.1.3 The NGI-ADPsoft model

The NGI-ADPsoft model is a user defined finite element model in PLAXIS 2D, developed as an extended version of the NGI-ADP model (Grimstad et al., 2010). The extended version was made with the intention of modelling strain softening behaviour of saturated clays during undrained loading (Andresen and Jostad, 2005; Grimstad and Jostad, 2012). The model is a plane strain total stress model that accounts for the anisotropy of the soil during undrained shearing (Grimstad and Jostad, 2012; Andresen and Jostad, 2002), which means that the soil behaviour depends on the direction of deformation (Fornes and Jostad, 2014). It is especially aimed at modelling normally- or lightly-overconsolidated saturated clay (Andresen and Jostad, 2002). The failure criterion is based on the Tresca yield criterion (Andresen and Jostad, 2002).

The purpose of NGI-ADPsoft is to avoid the mesh dependency that occurs when a finite element

model simulates strain softening behaviour. The problem with strain-softening in most finite element programs is the that refinement of mesh size causes increased brittleness of the soil and hence, mesh dependency occurs (Grimstad and Jostad, 2014). The NGI-ADPsoft model avoids the problem of mesh dependency by using the non-local strain approach proposed by Eringen (1981). The non-local approach is a regularisation technique (Brinkgreve, 1994) where the plastic strains are modelled by calculating an integrated average strain level limited in a defined region around a material point (D'Ignazio and Länsivaara, 2015; Grimstad and Jostad, 2014).

The model introduce an internal length parameter, l_{int}, that should be scaled according to the element size in the expected zone of softening (Grimstad and Jostad, 2014). Contributions within a radius of $3 \cdot l_{int}$ from a given material point is summed up when calculating the non-local strain increments (Grimstad and Jostad, 2014). This method avoids the dependence of mesh size, and instead obtain dependency of the deformation in a certain region (Grimstad and Jostad, 2012, 2014).

Brinkgreve (1994) discovered a problem with the non-local approach, namely that the calculated plastic strains concentrated and accumulated at the centre of the shear zone. Brinkgreve (1994) therefore developed the modified non-local approach with the intention of reducing the accumulated strain at the centre and thereby spreading the strains to the edges of the shear zone. The modified non-local approach introduced the parameter α in the non-local approach. By setting $\alpha = 1$, the formulation is the same as the non-local approach. The parameter has to be larger than one, $\alpha > 1$, to achieve an effective non-local regularisation (Brinkgreve, 1994). This approach is controlled by the two parameters α and l_{int} (Grimstad and Jostad, 2014). Jostad and Grimstad (2011) recommended to set $\alpha = 2$. l_{int} should be set equal to or larger than the element size in the failure region (Grimstad and Jostad, 2014). The softening parameters c_1 and c_2 value control the shape of the softening curve. The values are advised to be set equal to each other (Grimstad and Jostad, 2014).

Input parameters

The NGI-ADPsoft model requires several input parameters. These are results from triaxial compression, CAUc, and extension tests, CAUe, direct simple shear tests, DSS, and information about the initial stress condition, initial shear mobilisation and the elastic shear stiffness (Grim-

stad and Jostad, 2012). Figure 4.5 shows the required input parameters from the CAUc, CAUe and DSS tests. In table 4.4 in section 4.2.2 is the extended list of required input parameters given.

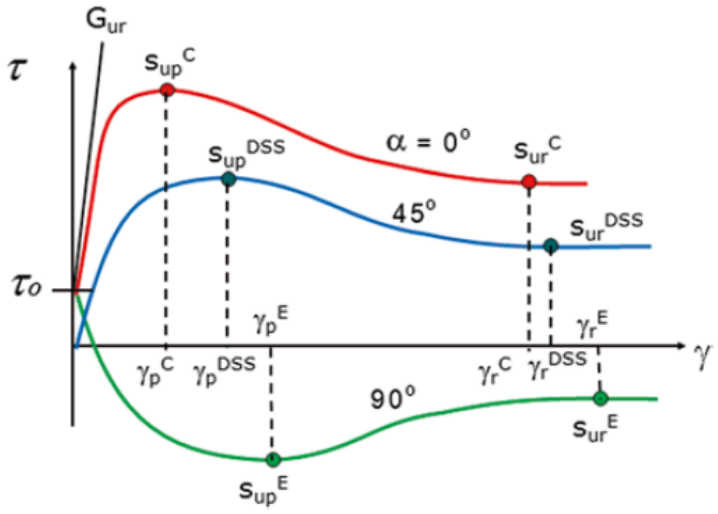

Figure 4.5: Input parameters for the NGI-ADPsoft material model from CAUc, CAUe and DSS tests, from Jostad et al. (2014).

Output

The NGI-ADPsoft model provides an output of three variable state parameters, respectively plastic shear strains, γ_p, a hardening parameter, κ_1 and a softening parameter, κ_2. The softening parameter is useful in terms of visualisation of the occurrence of strain-softening. The parameter is 0 at peak shear strength and 1 at residual shear strength. (Grimstad and Jostad, 2014)

4.2 Modelling approach

4.2.1 Geometry and boundary conditions

A model with arbitrary geometry was made for the simulations in PLAXIS, shown in figure 4.6. The slope was 15 m long with an inclination of 1:3. To avoid disturbances from the boundary conditions, a 30 m extension from the crest and backwards, and 30 m from the toe and forward was defined. The depth to bedrock was equal to 10 m for the entire model, thus the surface of bedrock followed the same inclination as at the surface of the slope. The installed pile was set 1

m from the crest of the slope, shown as the blue cluster in figure 4.6.

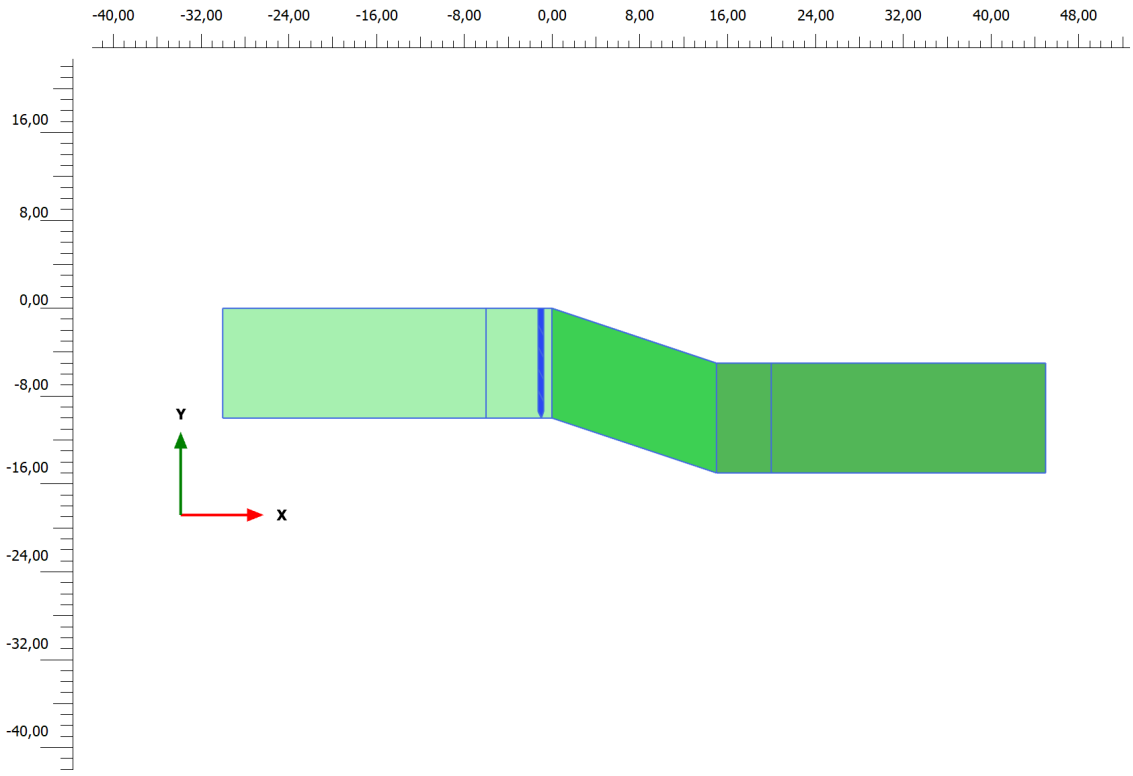

Figure 4.6: Model of the slope implemented in PLAXIS. The blue cluster at the crest of the slope is the simulated pile.

4.2.2 Soil profile

The soil profiles for the constitutive models were chosen to simulate a representative soil behaviour of a soft and sensitive clay material. Following are the input parameters for the three constitutive models, the Mohr-Coulomb model, the Hardening Soil model and the NGI-ADPsoft model.

General input parameters

General input parameters applied to all the constitutive models are shown in table 4.1.

Table 4.1: General input parameters used in all the different constitutive models.

Parameter	Unit	Description	Value
γ	kN/m^3	Soil density	18
e_{init}	-	Void ratio	0.5
ν'	-	Effective Poisson's ratio	0.3
K_0	-	Lateral earth pressure coefficient at rest	0.5

Input parameters of the Mohr-Coulomb model

Table 4.2 shows the input parameters for the Mohr-Coulomb model.

Table 4.2: Input parameters for the Mohr-Coulomb model.

Parameter	Unit	Description	Value
s_u	kPa	Undrained shear strength	$15+2\cdot z$
E'	kPa	Effective stiffness	10 000

Input parameters of the Hardening Soil model

Table 4.3 shows the input parameters for the Hardening Soil model.

Table 4.3: Input parameters for the HS-model.

Parameter	Unit	Description	Value
E_{50}^{ref}	kPa	Secant stiffness in drained triaxial test	10 000
E_{oed}^{ref}	kPa	Tangent stiffness for primary odeometer loading	10 000
E_{ur}^{ref}	kPa	Unloading/reloading stiffness	30 000
m	-	Power for stress-level dependency of stiffness	1
c'_{ref}	kPa	Effective cohesion	5
ϕ	[$^\circ$]	Friction angle	30
ψ	[$^\circ$]	Dilatancy angle	-1
OCR	-	Over-consolidation ratio	1.4

Input parameters in the NGI-ADPsoft model

The NGI-ADPsoft model had three different layers to achieve a continuous effective stress level that followed the surface of the slope. These are shown in table 4.4.

Table 4.4: Input parameters for the NGI-ADPsoft model. (Grimstad and Jostad, 2014)

Parameter	Unit	Description	Layer 1	Layer 2	Layer 3
G_{ur}/S_u^A	-	Normalised elastic shear modulus divided by undrained active peak shear strength	500	500	500
s_u^A	kPa	Undrained active peak shear strength at y_{ref}	15	15	15
${s_u}^A_{inc}$	kPa/m	Linear change of ${s_u}^A$ from y_{ref} with depth	2	2	2
x_{ref}	m	Horizontal reference position for y_{ref}	-30	0	18
y_{ref}	m	Reference depth for change of undrained shear strength	0	0	-5
$\Delta y_{ref}/\Delta x$	-	Change of y_{ref} as a function of x from x_{ref}	0	-0.333	0
$s_u^{DSS}/{s_u}^A$	-	Normalised undrained DSS peak shear strength	0.5	0.5	0.5
$s_u^P/{s_u}^A$	-	Normalised undrained passive peak shear strength	0.7	0.7	0.7
$s_u^A{}_r/{s_u}^A$	-	Normalised undrained active residual shear strength	0.3	0.3	0.3
${s_u^{DSS}}_r/s_u^A$	-	Normalised undrained DSS residual shear strength	0.3	0.3	0.3
$s_u^P{}_r/s_u^A$	-	Normalised undrained passive residual shear strength	0.3	0.3	0.3
τ_0/s_u^A	-	Initial shear mobilisation	0.25	0.25	0.25
γ_p^C	%	Shear strain at ${s_u}^A$	1.5	1.5	1.5
γ_p^{DSS}	%	Shear strain at ${s_u}^{DSS}$	1.5	1.5	1.5
γ_p^E	%	Shear strain at ${s_u}^P$	1.5	1.5	1.5
$\gamma_p^C{}_r$	%	Shear strain at $s_u^A{}_r$	15	15	15
$\gamma_p^{DSS}{}_r$	%	Shear strain at ${s_u^{DSS}}_r$	15	15	15
$\gamma_p^E{}_r$	%	Shear strain at $s_u^P{}_r$	15	15	15
c_1	-	Softening parameter 1	1	1	1
c_2	-	Softening parameter 2	1	1	1
ν_u	-	Undrained Poisson's ratio	0.495	0.495	0.495
α	-	Parameter for non-local strain	2	2	2
l_{int}	m	Internal length	Variable	Variable	Variable
INT. TYPE	-	Interpolation type for peak/residual strength	1	1	1

The internal length parameter, l_{int}, was scaled according to mesh size in the zone of the expected softening. The model was run with two different mesh discretisation, shown in the next

section. The model with the very fine mesh was defined with $l_{int} = 0.26$ m and the model with coarse mesh was defined with $l_{int} = 0.96$ m

4.2.3 Mesh properties

The Hardening Soil model and NGI-ADPsoft model were run with different mesh sizes, to study the effect of mesh-dependency. A general setting of very fine meshing was chosen, but by changing the coarseness factor, different discretisation of mesh size was determined. The mesh was refined in the areas where strain-softening expected to occur. These were cluster 2, 3 and 4, shown in figure 4.7. Whereas the outermost clusters, cluster 1 and 5, had coarser mesh to reduce calculation time. Cluster 1 and 5 were defined with a coarseness factor of 0.5 for all the models. Table 4.5 shows the chosen coarseness factors for the refined area for the constitutive models.

Table 4.5: Coarseness factors for the refined areas of mesh.

Model	Very fine mesh	Coarse mesh
Mohr-Coulomb	0.25	-
Hardening Soil	0.25	0.6
NGI-ADPsoft	0.15	0.5

The following figures shows the discretisation of mesh size for the constitutive models. Figure 4.7 and 4.8 shows the very fine mesh and coarse mesh for the Hardening Soil model, respectively. The Mohr-Coulomb model was run with the same mesh discretisation as the very fine mesh of the Hardening Soil model in figure 4.7. Figure 4.9 and 4.10 shows the very fine mesh and the coarse mesh for the NGI-ADPsoft model, respectively.

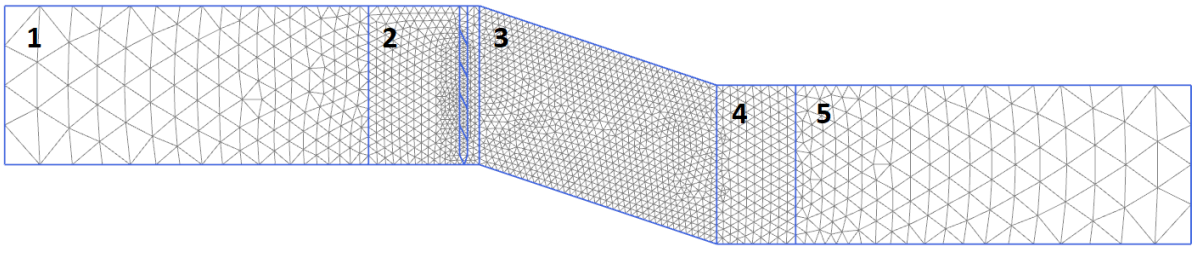

Figure 4.7: The very fine mesh for the HS-model and the Mohr-Coulomb model with numbered clusters.

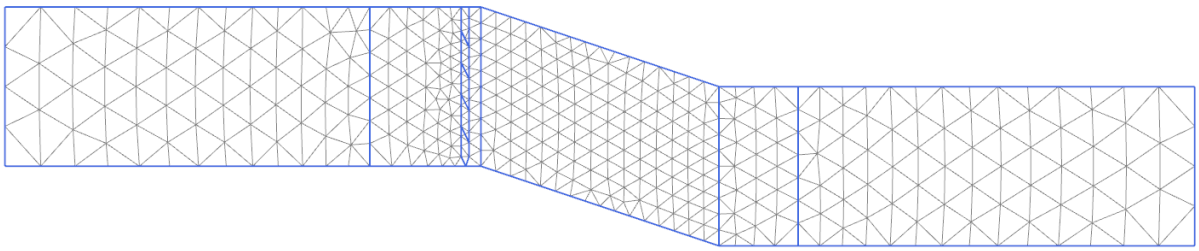

Figure 4.8: The coarse mesh for the Hardening Soil model.

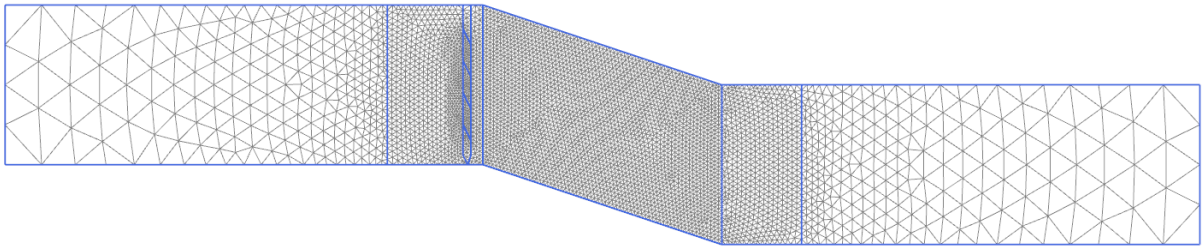

Figure 4.9: The very fine mesh for the NGI-ADPsoft model.

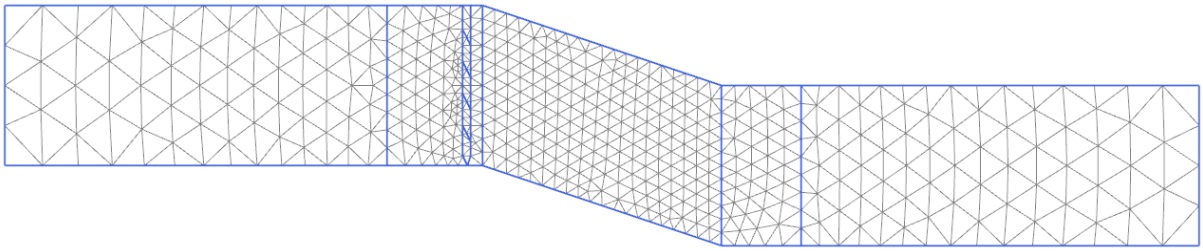

Figure 4.10: The coarse mesh for the NGI-ADPsoft model.

4.2.4 Drainage

The soil was assumed to be fully saturated, therefore the water level was set to follow the surface of the slope. PLAXIS offers different ways of defining the drainage type of the soil. The Mohr-Coulomb model was modelled with undrained B drainage type. The Hardening Soil model was modelled with drainage type undrained A, since it offers the possibility of defining dilatancy of the material. Undrained A uses effective parameters of strength and stiffness to model undrained behaviour (PLAXIS, 2019). Whereas undrained B uses undrained strength parameters and effective stiffness parameters to model undrained soil behaviour (PLAXIS, 2019). The NGI-ADPsoft model was defined with an general undrained setting.

During the PLAXIS simulations, a consolidation phase was run. Mainly with the intention to

consolidate the excess pore pressure that had accumulated during the activation of the soil gravity. The horizontal, k_x, and vertical permeability, k_y, was set equal to each other, shown in table 4.6.

Table 4.6: Permeability settings.

Parameter	Unit	Description	Value
k_x	[m/day]	Horizontal permeability	$1.0 \cdot e^{-5}$
k_y	[m/day]	Vertical permeability	$1.0 \cdot e^{-5}$

4.2.5 Method used to replicate pile driving

Pile driving was simulated by installing 0.5 m wide clusters down to bedrock at 1 m distance from the crest of the slope. The pile is shown as the blue cluster in figure 4.11. The material properties of the pile was the same as the surrounding soil, except that the drainage properties was set to drained.

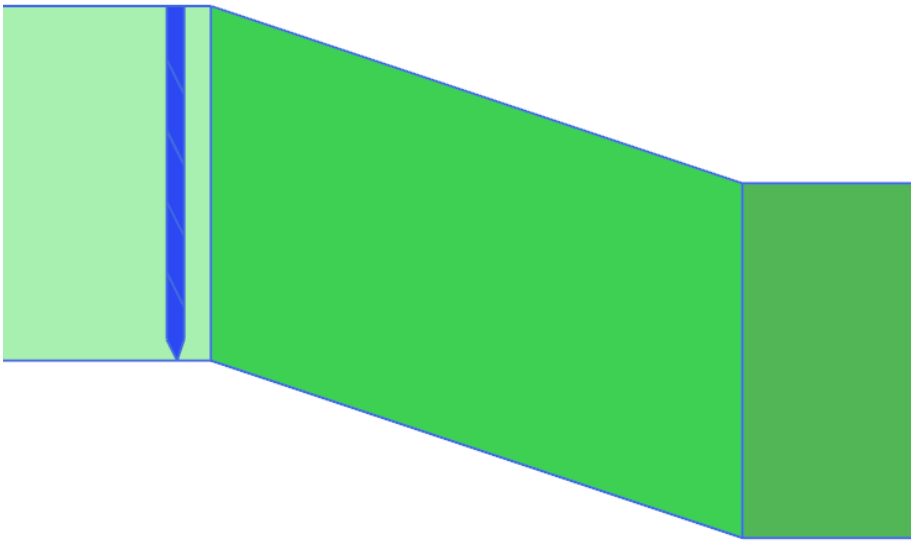

Figure 4.11: The figure shows the pile at the crest of the slope when fully installed down to bedrock. The pile is the blue clusters.

By dividing the pile into five volumes, it was possible to simulate a gradual installation of the pile down to bedrock. The gradual pile installation is illustrated in figure 4.12, numbered from step 1 to step 5. The mass displacement that occurs during pile driving was simulated by laterally expanding these clusters, by defining $\epsilon_{vol} = \epsilon_x = 15\%$. The steps was activated stepwise in

different phases in PLAXIS resulting in a gradual expansion of soil down to bedrock.

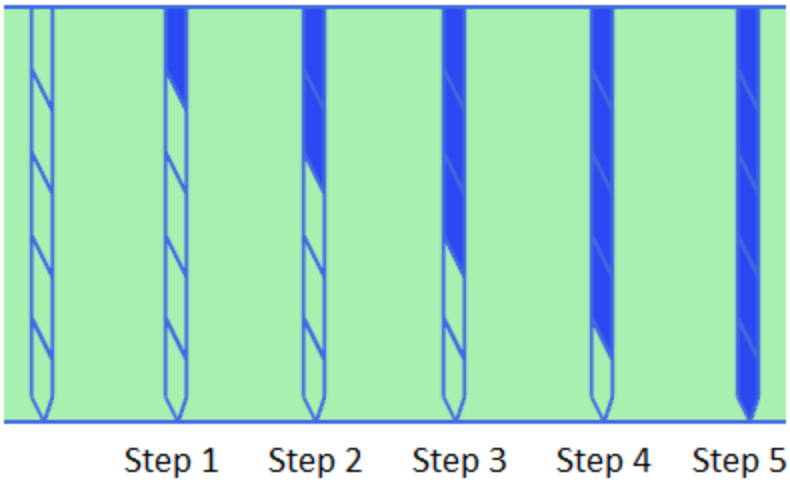

Figure 4.12: The steps simulating a gradual installation of a pile.

4.2.6 Calculation phases

Table 4.7 shows the general set up of calculation procedure for the constitutive models in PLAXIS.

Table 4.7: General calculation procedure in PLAXIS.

Calculation phase	Start from phase	Calculation type	Procedure
Initial phase		K_0 procedure	Generation of initial stresses.
Phase 1	Initial phase	Plastic	Activation of gravity of the soil.
Phase 2	Phase 1	Consolidation	Consolidation of generated excess pore pressure due to activation of gravity. Minimum excess pore pressure was set to 0.1 kPa
Phase 3	Phase 2	Plastic	Step 1. Activation of cluster 1 with the applied lateral strain.
Phase 4	Phase 3	Plastic	Step 2. Activation of cluster 2 with the applied lateral strain
Phase 5	Phase 4	Plastic	Step 3. Activation of cluster 3 with the applied lateral strain
Phase 6	Phase 5	Plastic	Step 4. Activation of cluster 4 with the applied lateral strain
Phase 7	Phase 6	Plastic	Step 5. Activation of cluster 5 with the applied lateral strain

The Hardening Soil with negative dilatancy suffered from model instability. To prevent the slope from failing during the activation of gravity, the initial phase and the activation of gravity phase, phase 1, had to be run with a material that was defined with zero dilatancy, $\psi = 0°$. An additional phase before the consolidation phase was added to change the material to the material with

negative dilatancy, $\psi = -1.0°$.

In addition to the phases in table 4.7, were the Mohr-Coulomb model and the Hardening Soil model run with a safety phase in PLAXIS. The safety phase is not applicable for the NGI-ADPsoft model, so this procedure could not be conducted for this model. The Mohr-Coulomb model was run with a safety phase before and after the simulated pile driving. The intention was to see whether the simulations affected the stability of the slope.

This approach could not be conducted for the Hardening Soil model. Since the model experienced numerical issues and would not converge during the safety phase when the soil had negative dilatancy. The solution became to run a safety phase with a material with the same properties as in table 4.3, but changing the dilatancy angle to zero, $\psi = 0°$. A sense of the stability situation could then be obtained. However, the stability phase could not be run after the pile driving simulations, since the material for these phases had negative dilatancy.

Chapter 5

Results

This chapter includes the results from the conducted analyses. The presented results are the achieved results from the Mohr-Coulomb model, Hardening Soil model and NGI-ADPsoft model.

5.1 The Mohr-Coulomb model

The effect of pile driving in the vicinity of a slope was firstly studied in a perfectly plastic Mohr-Coulomb model. The safety calculations in PLAXIS showed that the slope stability was unchanged after the simulated pile driving, resulting in an unchanged factor of safety to 2.02 before and after pile installation.

5.1.1 Evaluation of the Mohr-Coulomb model

The Mohr-Coulomb model did not give the desired effects in terms of a reduced slope stability situation after the simulated pile driving. As mentioned in the introduction, an increase of pore pressure in an undrained elasto-plastic total stress model does not affect the effective stress situation and as a result soil strength remains unchanged. With no change in the soil strength, such simulations do not provide a reduction in the factor of safety of the slope during pile driving and cannot represent any failure mechanism. It was therefore deemed necessary to try more advanced models to capture the effect of volume expansion on slope stability. The choice fell further on the Hardening Soil model which is a more advanced model than the Mohr-Coulomb model.

5.2 The Hardening Soil model

The following section presents the results from the Hardening Soil model in PLAXIS. Two models were run, one with very fine mesh and one with a coarser mesh, shown in figure 4.7 and 4.8, respectively.

Before the simulations of pile driving started, a safety calculation phase was run in PLAXIS. As mentioned in section 4.2.6, the phase was run with a material with zero dilatancy. The analysis resulted in a factor of safety to 1.32, which gave an idea of the safety level of the slope before pile driving started.

5.2.1 Very fine mesh

The simulated pile driving for the model with very fine meshing triggered a slope failure. Failure occurred during step 2 of the pile driving simulations. Figure 5.1 shows the soil collapse.

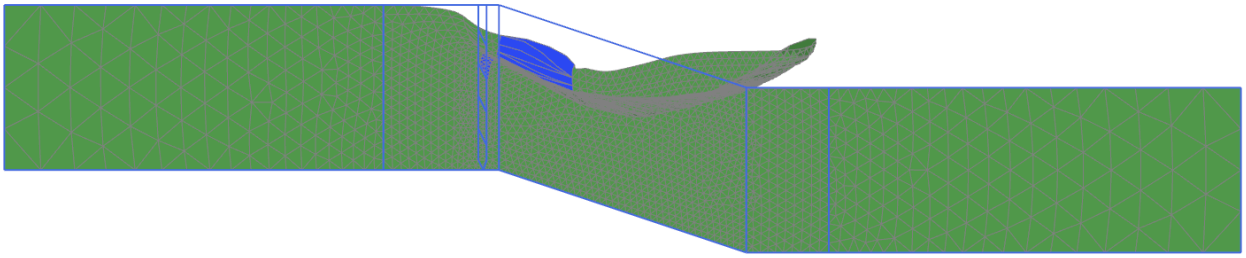

Figure 5.1: Soil collapse due to the simulated pile driving scaled up 5 times.

Figure 5.2 shows the failure mechanism in terms of the shear strain distribution at failure. The points A, B, C, D and E were selected stress points for plotting of shear stress-strain relationships.

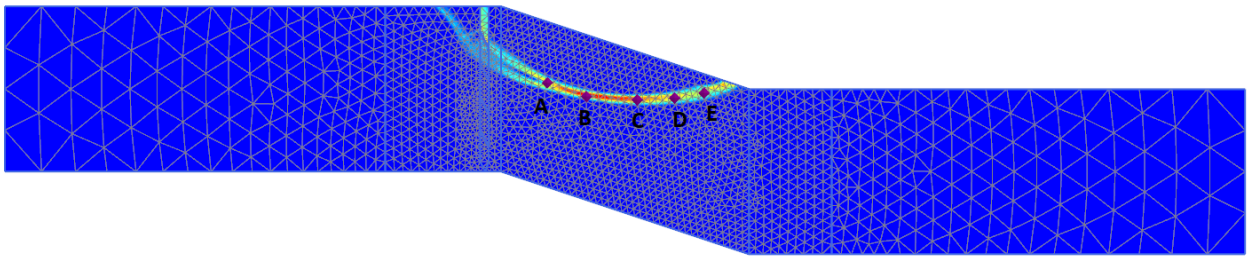

Figure 5.2: Failure mechanism in terms of the shear strain distribution. The points A, B, C, D and E were selected points for plotting of shear stress-strain relationships.

The distribution of mobilised shear stress, τ_{mob}, plotted with shear strains, γ_S, through the steps

of the simulated pile driving are shown in figure 5.3 for the selected points A-E. The shear stress reached a distinct peak for the different points at an approximate $1-2\%$ strain level. Point B, situated nearly in the middle of the slip surface, attained the highest shear stress to 16 kPa. After peak stress was reached, the shear stresses reduced quite rapidly between strain levels of $5-20\%$. The curves were quite similar to each other, in terms of following the same negative inclination towards a constant stress level. At strain levels between $15-23\%$, the selected points quite suddenly stopped reducing at the same constant shear stress, $\tau_{mob} = 8.66$ kPa. The shear stress-strain curves continued to follow this constant shear stress with increasing strains.

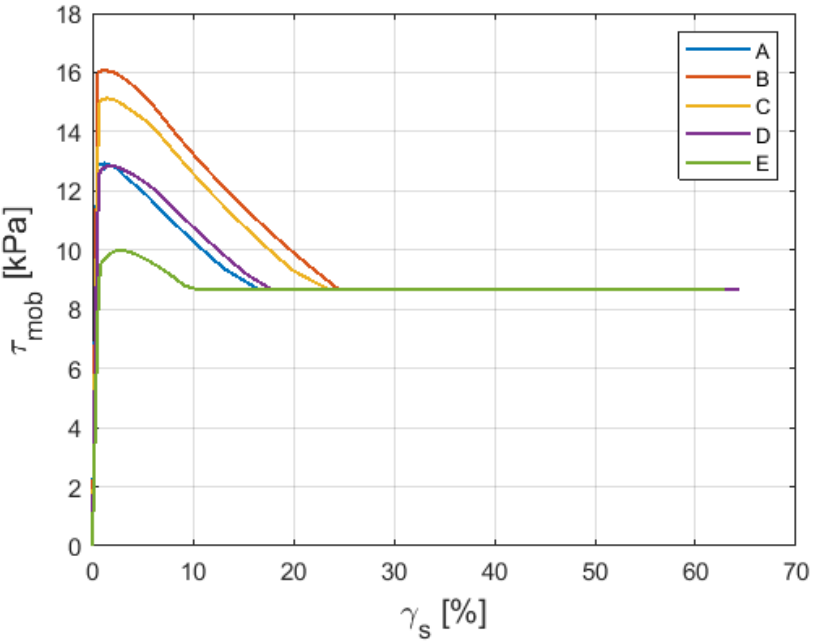

Figure 5.3: Shear stress-strain propagation for the points A, B, C, D and E given in figure 5.2.

Figure 5.4 shows the propagation of the failure mechanism as it developed through the slope. The onset of the shear strains is shown in figure 5.4a, for strain levels that corresponded to the situation just passed the peak shear stress. The propagation of a shear surface is displayed in figure 5.4b, with strain levels referring to the state of rapid loss of shear stress, shown in figure 5.3. Slope failure occurred when a continuous mechanism had propagated through the slope, shown in figure 5.4c. These strain levels referred to the state where the soil had attained the constant shear stress.

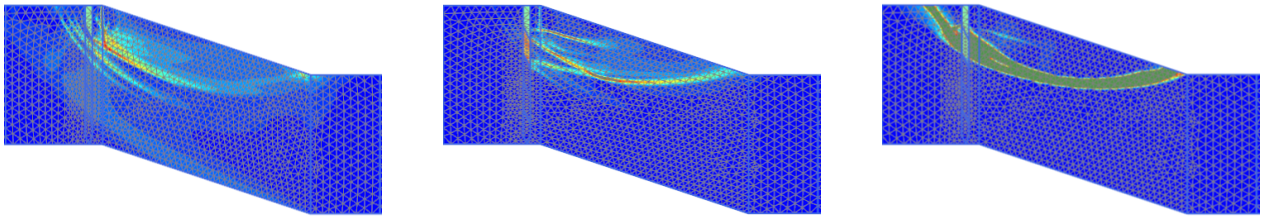

(a) Onset of shear strains. (b) Propagation of the shear strains. (c) Failure mode.

Figure 5.4: Propagation of failure mechanism in terms of the shear strain distribution. For better visualisation of distribution patterns, strains shown on the legend are limited to 2% on figure (a), to 10% on figure (b) and to 25% on figure (c).

In figure 5.5, shear stress is plotted with the steps of the simulations. Step 2 marks the transition between step 1 and step 2 of the simulated pile driving. The black dots visualise that the different points reached peak shear stress at the order of A, B, C, D and E. Point A reached constant shear stress first, followed by point E and lastly the remaining points.

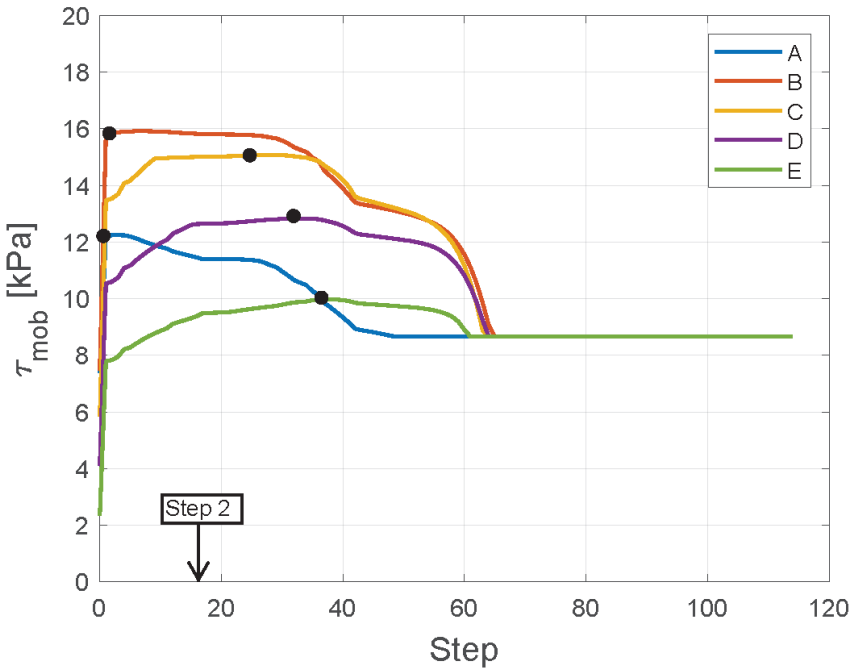

Figure 5.5: Shear stress plotted with the steps during the simulations. The black dots marks the attained peak stress for the respective points. Step 2 mark the transition between step 1 and step 2 of the simulated pile driving.

The excess pore pressure distribution in failure mode is shown in figure 5.6. The selected points A-E is shown to visualise the position of the failure mechanism in figure 5.2. These points shows that a local increase of excess pore pressure occurred in the same area as the developed critical

surface. The soil outside this failure surface had little generation of excess pore pressure.

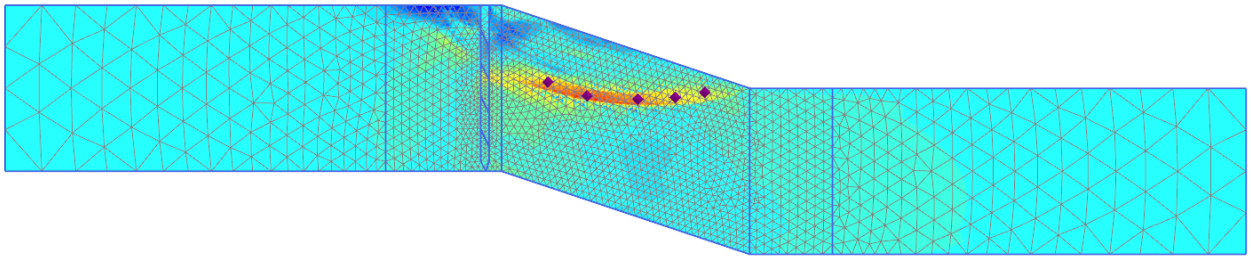

Figure 5.6: Excess pore pressure distribution in failure mode. The selected points A-E is shown to visualise the position of the failure mechanism in figure 5.2

5.2.2 Coarse mesh

The model with coarse mesh did not experience failure due to the simulated pile driving. Figure 5.7 shows the deformed mesh after the analysis had run through, showing that little deformation occurred.

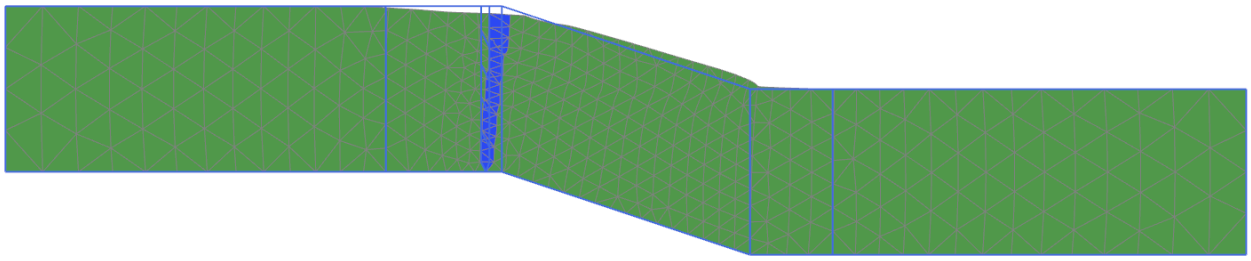

Figure 5.7: Deformations after the simulated pile driving scaled up 5 times.

Figure 5.8 shows the shear strain distribution after the mass displacements from pile driving. There seem to be a progressing mechanism with higher levels of developed strain.

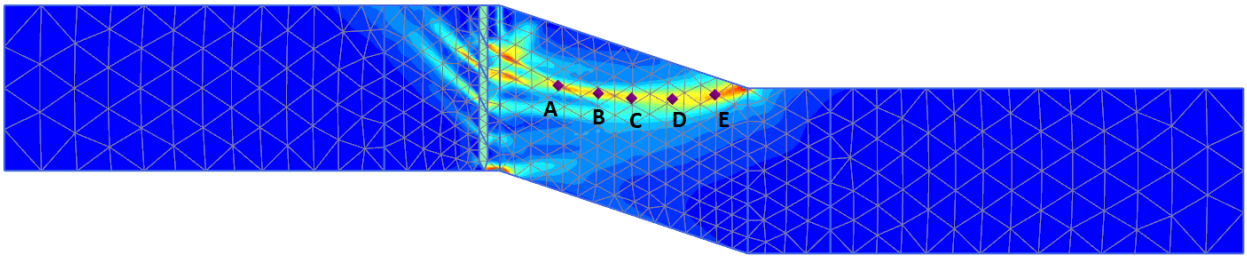

Figure 5.8: Shear strain distribution after the simulated pile driving. The points A, B, C, D and E were selected points for plotting of shear stress-strain relationships.

The shear stress-shear strain propagation during the simulations are plotted in figure 5.8 for

the selected points A-E. The soil reached its peak shear stress at a 0.5 – 0.7% strain level. With increasing strain levels, the mobilised shear stress remained close to constant.

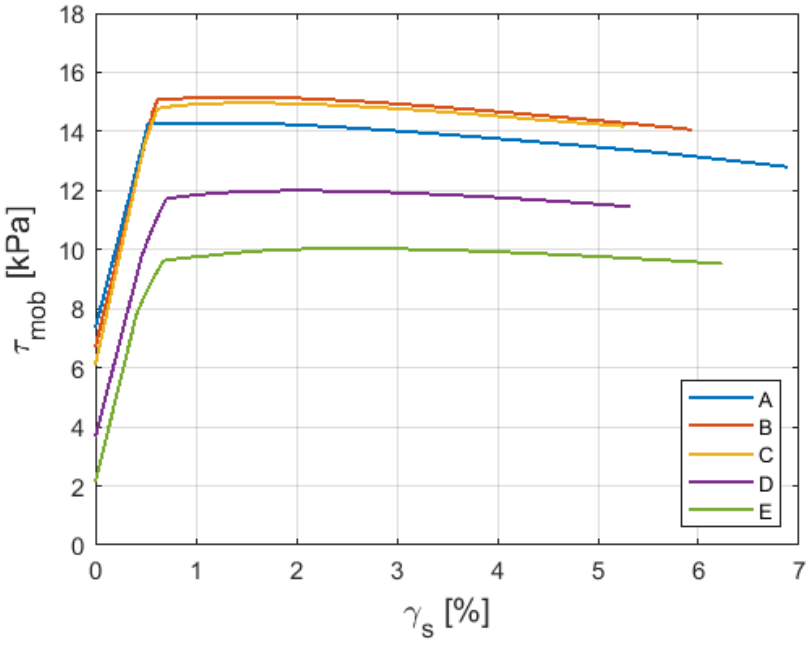

Figure 5.9: The shear stress-shear strain propagation during the simulation for the selected points A-E in figure 5.8.

The onset of shear strains is shown in figure 5.10a, for strain levels referring to the situation passed the peak stress in figure 5.9. Following, in figure 5.10b, the distribution of shear strains after the last step of the simulations is shown. A more evident surface had occurred for strain levels up to 7%, but no failure occurred.

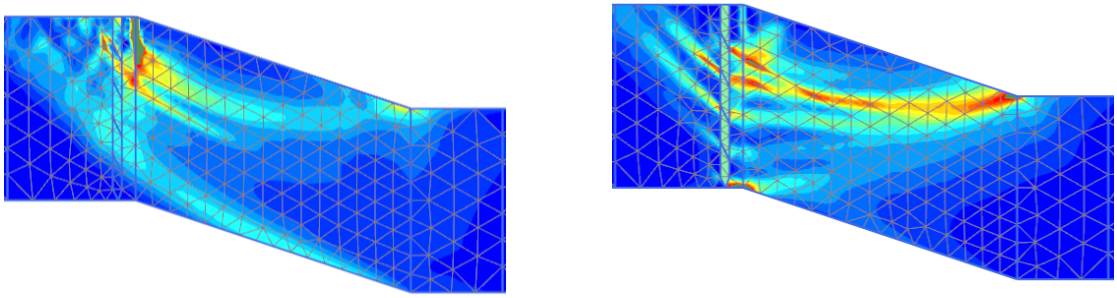

(a) Onset of shear strains.

(b) Distribution of shear strains after ended analysis.

Figure 5.10: Propagation of shear strains. For better visualisation of distribution patterns, strains shown on the legend are limited to 1.5% on figure a and to 7% on figure b.

The excess pore pressure distribution is shown in figure 5.11. The excess pore pressure mainly

generated by the tip of the pile. There were little accumulation of excess pore pressure inside the developing mechanism, visualised by showing the positions of the selected points.

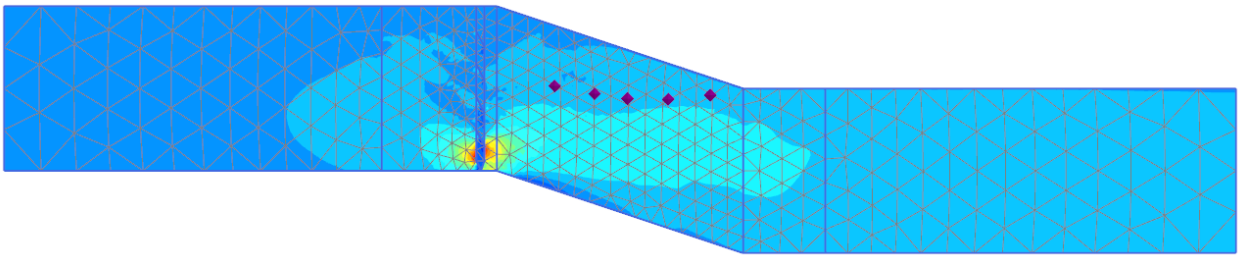

Figure 5.11: Excess pore pressure distribution after simulated pile driving. The selected points are shown to visualise the position of the developing mechanism in figure 5.8.

5.2.3 Evaluation of the Hardening Soil model

The HS-model had major limitations in terms of mesh dependency. This was visualised by running two models with different mesh coarseness, one with very fine mesh and one with a coarser mesh. The outcome of the simulations were very different depending on the choice of meshing, whereas the model with very fine mesh initiated slope failure and the model with coarse mesh did not. The HS-model also suffered from instability problems. Both the initial and gravity phase of the simulations had the be run with a material with zero dilatancy. An additional phase with changing to a material with negative had to be added before the consolidation phase in PLAXIS. Considering the mesh dependency and the model instability, it was therefore deemed necessary to look for another model that could simulate these types of behaviour in a more sufficient way. After some research, and studying several relevant articles (e.g. Andresen and Jostad (2002); Grimstad and Jostad (2014, 2012); Grimstad et al. (2010); Jostad and Grimstad (2011); D'Ignazio and Länsivaara (2015)), the NGI-ADPsoft model seemed to be the model to represent this mechanism more realistically.

5.3 The NGI-ADPsoft model

In the following section, the results from the NGI-ADPsoft model are presented. Two models with different mesh sizes, shown in figure 4.9 and 4.10, with the internal length parameter scaled according to mesh size, were run.

5.3.1 Very fine mesh

The following results comes from the model with very fine mesh and $l_{int} = 0.26$ m. The simulated pile driving initiated failure during step 3 of the pile driving simulations. Figure 5.12 shows the soil collapse of the slope.

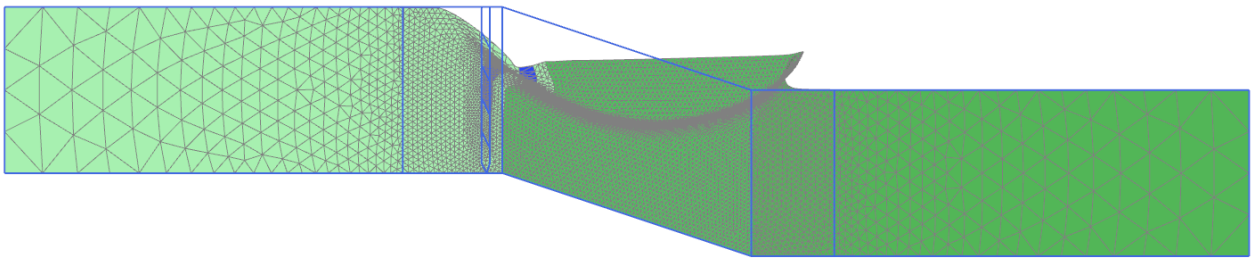

Figure 5.12: Soil collapse scaled up 5 times.

Figure 5.12 shows the failure mechanism of the slope in terms of the distribution of shear strains. The critical failure surface was a toe circle, which means that the failure surface ended at the toe of the slope.

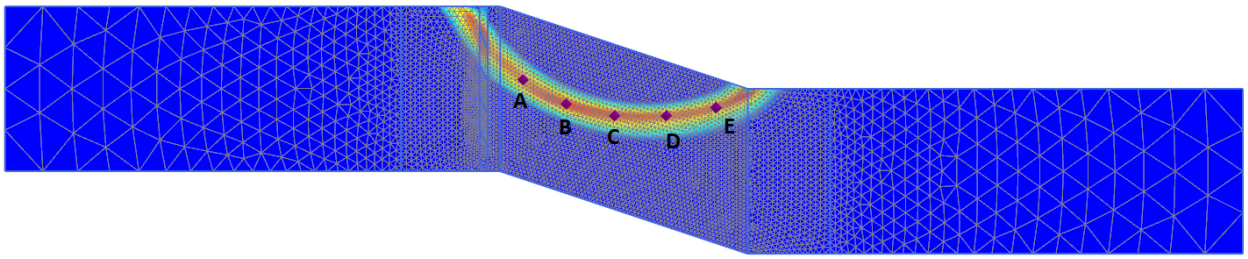

Figure 5.13: Shear strain distribution in failure mode. A, B, C, D and E were selected points for plotting of stress-strain relationships.

The shear stress-shear strains propagation are plotted in figure 5.14 during simulated pile driving. The curves reached a distinct peak shear stress at $1-1.5\%$ strain level. Point A, B and C had quite similar peak shear stress to around $\tau_{mob} = 20$ kPa, whereas point D and E had significantly lower peaks at $\tau_{mob} = 15$ kPa and $\tau_{mob} = 11$ kPa, respectively. After the peak was reached, the shear stresses decreased rapidly with increasing levels of strains. From a 15% strain level, the decreasing of shear stress stopped and remained constant for further increasing strain. Curve A, B, C and D, attained a similar constant shear stress to around 7 kPa. Curve E had somewhat lower constant shear stress to 5,5 kPa.

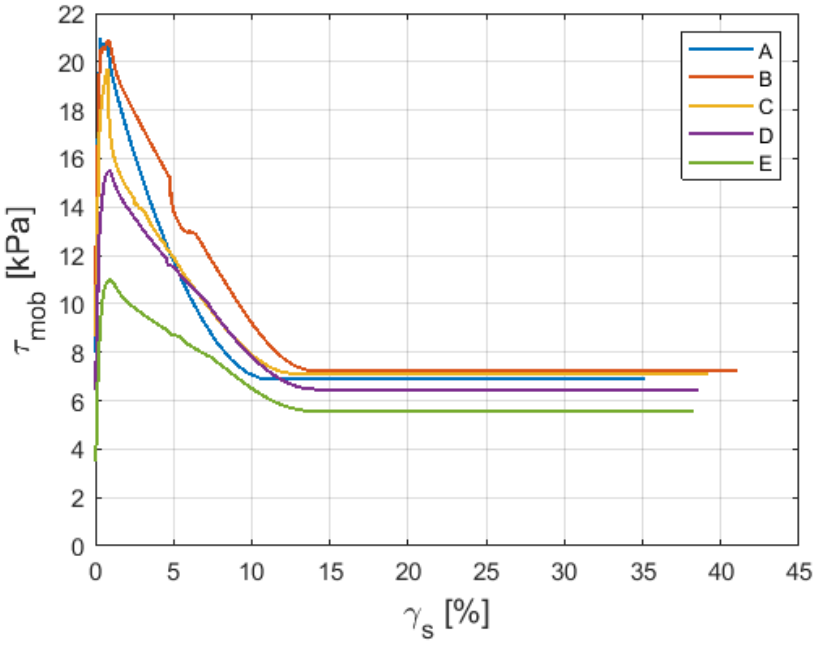

Figure 5.14: Shear stress-shear strain propagation during the simulations plotted for the selected points A, B, C, D and E, given in figure 5.13.

The distribution of the softening parameter, κ_2, is shown in figure 5.15. Red contours shows areas where $\kappa_2 = 1$, referring to a state where the soil had reached the residual stage, and the shear strength was equal to the residual shear strength. The blue contoured area, $\kappa_2 = 0$, were areas where the soil remained at its peak strength. The area with residual strength followed the same thickness as the distinct band of increased levels of strains in figure 5.13.

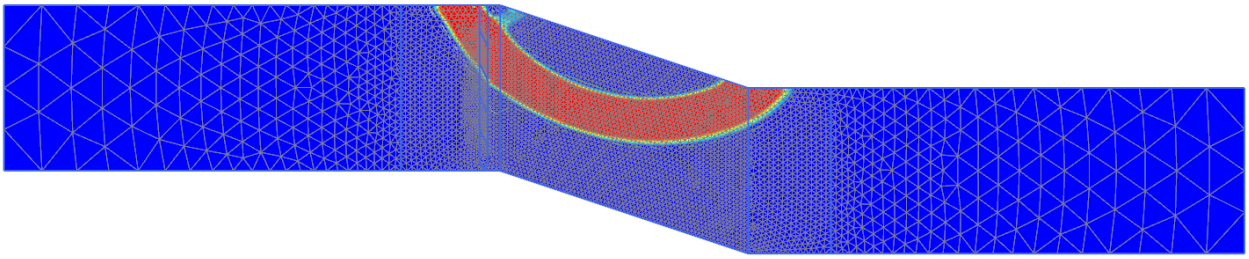

Figure 5.15: Contours of the softening parameter κ_2. The red shadings were areas where the shear strength had reached the residual shear strength, $\kappa_2 = 1$. The blue shadings are areas where the soil remained at its peak strength, $\kappa_2 = 0$.

The propagation of the failure mechanism is shown in figure 5.16. Figure 5.16a shows the strain localisation of the mechanism. The onset occurred beneath the crest of the slope, for strain levels corresponding shear stress that had just passed the peak. Further, in figure 5.16c, the propa-

gation of the failure surface is visualised. Referring to the situation with rapidly decreasing shear stress, shown in figure 5.14. Ultimately, the failure mechanism is shown in figure 5.16c, where a distinct band of high levels of shear strains had occurred. The soil inside the distinct band had reached strain levels well above 20%, which means that the soil had reached the constant value of shear stress, shown in figure 5.14.

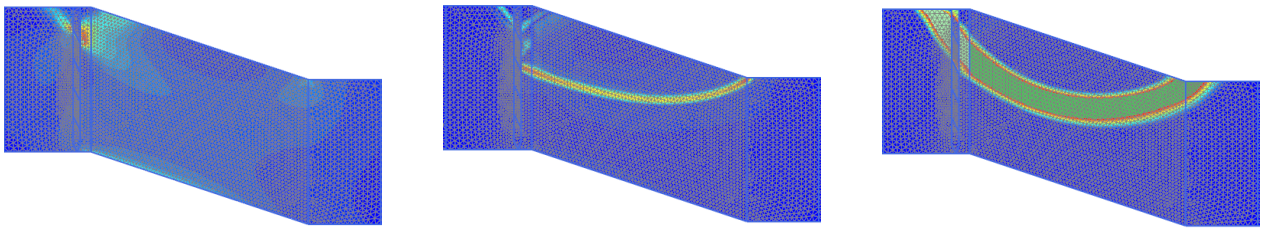

(a) Onset of shear strains. (b) Propagation of the shear strains. (c) Failure mode.

Figure 5.16: Propagation of failure mechanism in terms of the shear strain distribution. For better visualisation of distribution patterns, strains shown on the legend are limited to 2% on figure a, to 7% on figure b and to 20%.

Figure 5.17 shows the propagation of shear stress plotted with the steps of the simulations. The black dots visualise the step at which the selected points reached its peak shear stress during the simulations. Point A reached a peak at step 26. Compared to the other points, it had a irregular shear strength propagation. Point B reached the peak at step 51 and point C, D and E reached the peak simultaneously during step 59. The constant shear strength was reached at approximately the same step, at step 184.

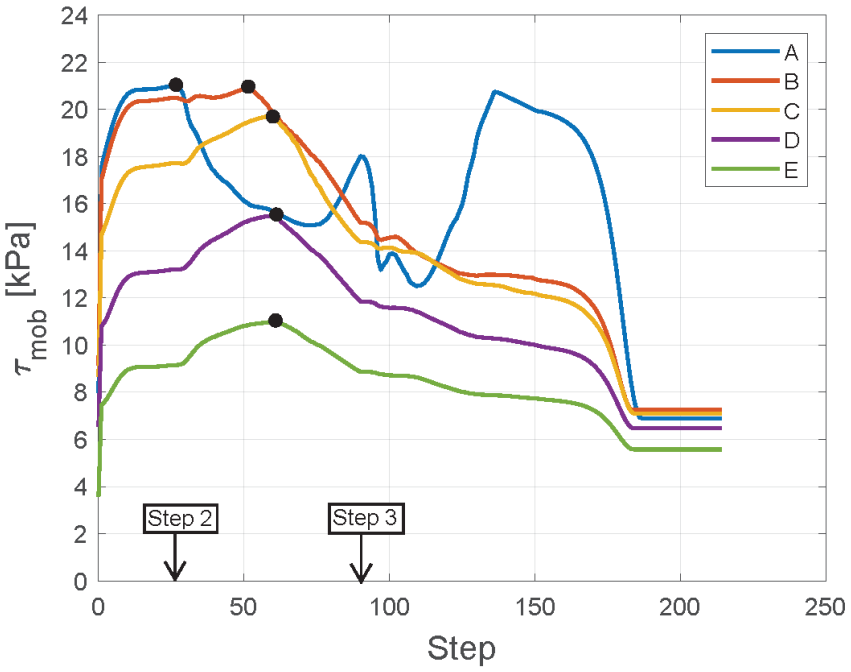

Figure 5.17: Shear stress plotted with the steps during the simulations. Step 2 and step 3 refer to the starting point of the respective pile driving steps. The black dots mark where the selected points reached peak stress.

5.3.2 Coarse mesh

The NGI-ADPsoft model with coarse mesh and l_{int} = 0.96 m did not initiate failure during the simulated pile driving. Figure 5.18 shows that the simulations resulted in little deformation of the slope.

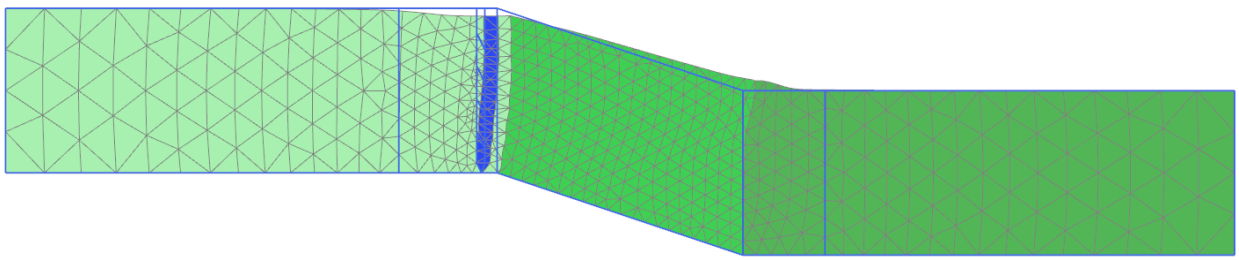

Figure 5.18: Deformed mesh after the simulated pile driving scaled up 5 times.

The shear strain distribution after the simulated pile driving is shown in figure 5.19. There seem to be a progressing mechanism with higher levels of developed strain.

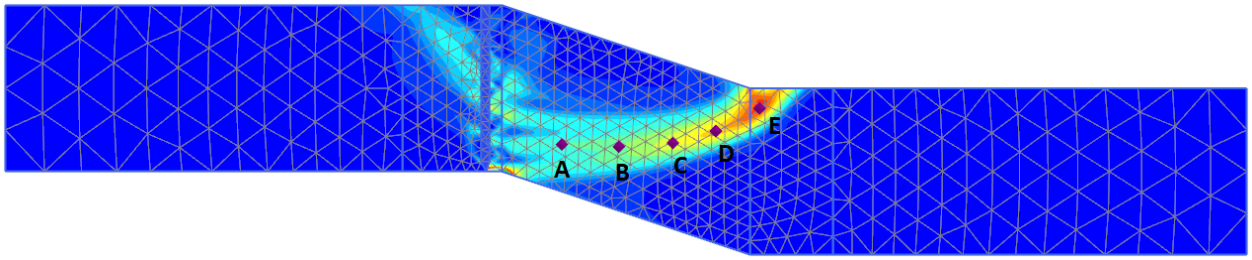

Figure 5.19: Shear strain distribution after the simulated pile driving. Point A, B, C, D and E were selected for plotting of the shear strength-strain relationships. Strains shown on the legend are limited to 6%.

The propagation of mobilised shear stress with shear strains are plotted for point A-E in figure 5.20 through pile driving simulations. Point A, B and C had distinct peak shear stresses at strain levels between $0.4-0.6\%$. A sudden drop of shearing resistance occurred after the peak for these points. In contrary to point D and E, which after reaching a peak shear strength, had a very weak reduction of shear stress with increasing strain. For point A, B and C, at strain levels between $0.6-0.9\%$, the shear stresses stopped reducing with such rapidness and started to follow the same weak inclination as for point D and E.

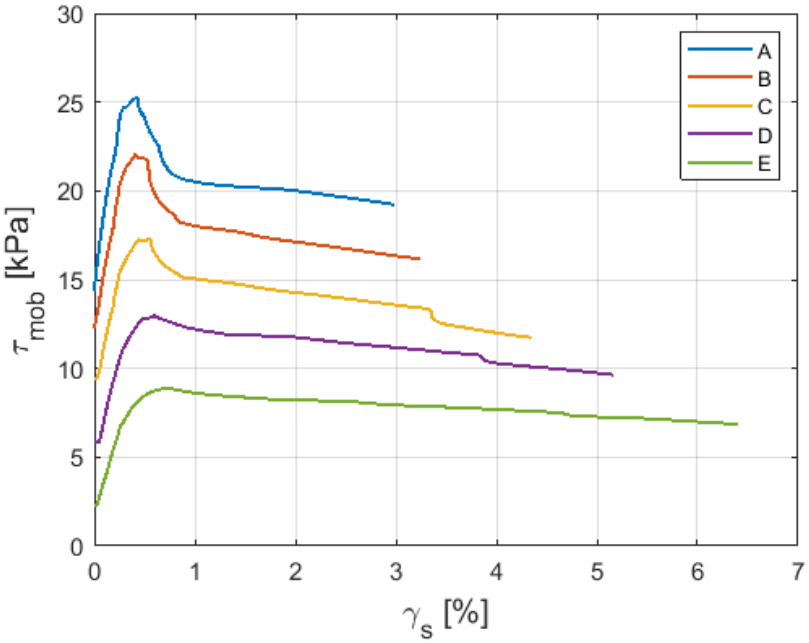

Figure 5.20: Shear stress-shear strain propagation during the simulations plotted for the selected points A, B, C, D and E, given in figure 5.19

Figure 5.21 shows the progression of shear strains in two steps, the onset of shear strains and the

distribution of shear strains at end of the simulations. The localisation, i.e. the red contours, in figure 5.21a showed strain levels referring to the state where the shear stresses that had passed the peak. A more evident mechanism had developed in figure 5.21b, but no failure occurred.

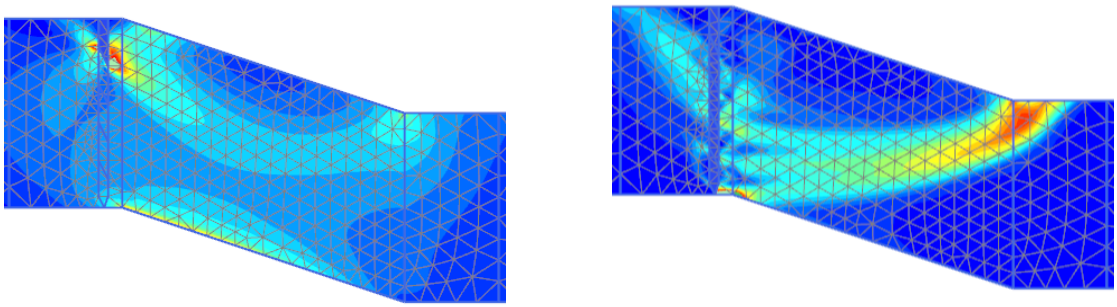

(a) Onset of shear strains.

(b) Propagation of shear strains after the simulated pile driving.

Figure 5.21: Propagation of shear strains. For better visualisation of distribution patterns, strains shown on the legend are limited to 1.0% on figure a and to 7% on figure b.

Contours of the softening parameter, κ_2, between 0 and 1 are shown in figure 5.22. No areas in the slope experienced full softening, in terms of reaching the residual state at $\kappa_2 = 1$.

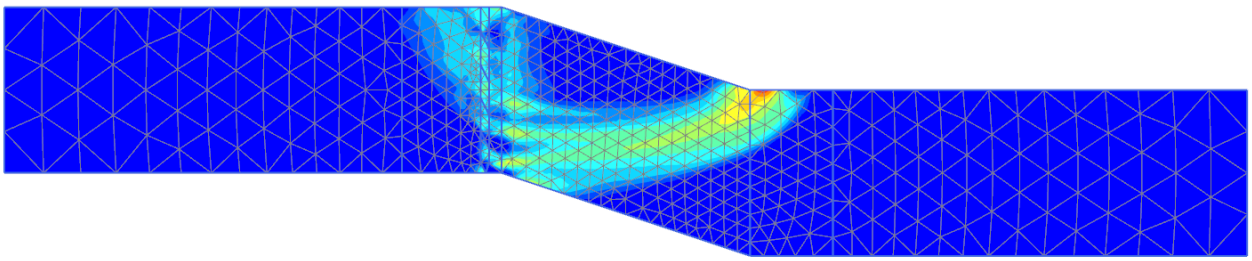

Figure 5.22: Contours of the softening parameter κ_2, limited in the range from 0 to 1.

Chapter 6

Discussion

The work with this thesis was set out to answer the following research questions: Can finite element methods simulate the strain-softening of the soil material during pile driving? Can a simulation of pile driving in a finite element program initiate a progressive failure mechanism? These questions will in the following chapter be discussed in terms of the obtained results from the simulations in PLAXIS.

The purpose of the finite element simulations was to model a slope failure due to pile driving nearby the crest of a slope. The goal was therefore that the analyses should not be able to complete entirely, as the slope should fail due to the disturbances from the pile driving initiating a progression of strain-softening behaviour.

6.1 The Mohr-Coulomb model

The Mohr-Coulomb model did not grant the desired effects in terms of reduced slope stability, and ultimately slope failure, during the simulation. The factor of safety was unchanged after the simulated pile driving. Due to the elastic perfectly plastic soil behaviour, the model was not able to simulate a strain-softening response. The model generated excess pore pressure from an increase in the total mean stress situation (PLAXIS, 2019). As previously stated, an increase of excess pore pressure due to the increase in total mean stress will not affect the effective stresses. Consequently, the shear strength remains unchanged and no reduction in slope stability.

6.2 The Hardening Soil model

The model with very fine mesh, initiated failure during step 2 of the simulated pile driving. Contrary to the model with coarse mesh that could run through the simulations without initiating failure. The results from the model with very fine mesh is mainly discussed in this part, since it lead to the wanted result in terms of slope failure.

6.2.1 Strain-softening behaviour

The model with very fine meshing was able to simulate a loss of shear stress when subjected to shear deformations induced by the simulated pile driving. This loss of mobilised shear stress was provoked with the use of a negative dilatancy angle. The shear stress-strain curves in figure 5.3 shows that the curves reached a distinct peak shear strength before it had a significant loss of shearing resistance at strain levels between 5−23%. When the soil reached shear stress to $\tau_{mob} =$ 8.7 kPa, the shear stresses suddenly stopped reducing and became constant with increasing strain, resembling a residual shear strength.

Since the model obtained a peak shear strength, followed by a post-peak phase of reduced shear stress and lastly a residual shear strength, it can be concluded that the model sufficiently managed to model a strain-softening response. Obtaining a shear stress-strain behaviour that was quite similar to the softening curves of brittle soils. However, the strain-softening curve had a quite sudden stop of the decreasing shear stress towards the state of constant shear stress. It lacked the smooth transition between the two states of decreasing and constant shear stress.

The decrease in shear stress came seemingly from the contractive behaviour generating shear-induced excess pore pressure, further leading to a reduction of effective stresses. The end of contracting behaviour was controlled by the tension cut-off function. It seemed that when the shear strength that originated from the friction angle had diminished, the contractive behaviour stopped. The remaining shear strength at the residual phase came seemingly from the cohesion of the soil. If the tension cut-off had not been activated, the shear stresses would have reduced towards zero by diminishing the contribution from cohesion as well. This behaviour was shown in figure 4.4 with the use of the soil test function in PLAXIS.

The model with coarse mesh had a shear stress-strain propagation that resembled more towards an elastic perfectly plastic soil behaviour, shown in figure 5.9. The lack of strain-softening

behaviour was presumably the reason that the model did not initiate failure. Since the shear stresses remained close to constant with increasing strain after reaching the peak strength, the simulations had little effect on slope stability.

6.2.2 Progressive failure

To study whether the model was able to simulate a progressive failure mechanism, the shear strain propagation was visualised at three steps during the simulations, shown in figure 5.4. The figures show that the soil attained different phases during the strain-softening process. First, a shear localisation where the soil had reached the peak strength. Secondly, the development of a shear surface for strain levels between 5 – 15%, corresponding to the state of rapid decreasing shear stresses. Lastly, the failure mode with strain levels well above 25%, referring to the state of residual shear strength. Based on these figures, it may seem like there was a progressive manner to the failure propagation.

Studying the propagation of shear stresses with the steps during the simulations in figure 5.5, it is possible to see that point A, B, C, D and E reached the peak shear strength at different steps following each other. The residual strength was first reached by point A, followed by point E, and lastly the remaining points approximately during the same step. This may suggest that the strain-softening propagated progressively, since the points reached the peak and residual at different times.

However, the illustration by Andresen and Jostad (2007) in figure 3.3 shows a clear visualisation of how a progressive failure mechanism would ideally look like. In this illustration, the soil had attained different phases of the strain-softening process throughout the slope, visualised by one part of the soil in residual state while other parts were at the peak or still in the pre-peak state. The simulations did not show this domino-effect that could describe a progressive failure.

Since the selected points reached the peak and residual state at different steps, it can hence be said that the simulations with the HS-model and very fine meshing showed tendencies of progressive failure.

6.2.3 Shear bands

From the shear strain distribution in figure 5.2 it is possible to see the development of a distinct band of increasing levels of strain. Most of the shear strains at failure occurred and accumulated within this band and little occurred at the outside, which resembles what happens inside a shear band. However, the difference became in terms of the thickness of the bands. The developed band expanded over approximately two elements, resulting in a thickness of 0.56 m. In a real clay soil, the shear band thickness may be only millimetres thick. Thakur (2007) found the shear band to be 3.0 to 4.0 mm at the onset of strain localisation. The shear band may however only be a hairline thin (Grimstad et al., 2005).

As mentioned in the theory section, the development of shear bands creates a non-uniform distribution of excess pore pressure, resulting in an increase of excess pore pressure inside the shear band, and ideally no generation outside (Gylland et al., 2014). Figure 5.6 shows a significant increase of excess pore pressure inside this band. Since the model was able to account for contractive soil behaviour, the model produced shear-induced excess pore pressure in addition to the increase of excess pore pressure from an increase in total mean stress.

The coarse mesh model gave less of the mentioned effects. Figure 5.8 shows that there was a developing shear surface due to the simulated pile driving. But the shear deformations were not great enough to initiate a strain-softening response. Excess pore pressure did not accumulate inside the developing band as it did for the model with very fine mesh. Instead, the excess pore pressure increased beside the tip of the pile near bedrock.

6.2.4 Limitations of the Hardening Soil model

Simulations from the HS-model with negative dilatancy clearly showed that the model held mesh-dependent properties. As the mesh was refined, less of the simulations were able to run through. The very fine mesh model resulted in slope failure during step 2 of the simulations. Whereas the coarse mesh model could complete the analysis with no failure occurring. This makes the HS-model with negative dilatancy unfit to simulate strain-softening behaviour for the purpose of geotechnical engineering.

The fact that the use of negative dilatancy angle resulted in an instability of the model was experienced. Small external disturbances lead to collapse or numerical issues stopping the model

from running. Further, it also experienced to be important that all excess pore pressure due to the appliance of soil gravity was dissipated before the simulated pile driving could start. If this was left out, the model collapsed nearly before the simulation of pile driving started.

6.3 The NGI-ADPsoft model

The NGI-ADPsoft model was able to trigger failure due to the simulated pile driving for the model with very fine mesh. However, the model with coarse did not experiencing failure, as it could complete the analysis entirely. The following section is therefore primarily based on the results from the model with very fine meshing, unless otherwise stated.

6.3.1 Strain-softening behaviour

The shear stress-strain curves of the selected points A-E in figure 5.14 for the model with very fine meshing, shows that the model managed to simulate a strain-softening effect that resembled the results from a triaxial test of brittle soil. The softening curves showed a distinct peak shear strength, before it experienced a significant loss of shearing resistance, in the post-peak phase. At shear strain levels above 15%, the shear stresses attained a constant residual shear strength with increasing strain. Since the model managed to simulate a peak shear strength, followed by a rapid reduction of shear strength and lastly reaching a residual strength, it can hence be concluded that the NGI-ADPsoft model successfully simulated strain-softening behaviour initiated by pile driving.

On the contrary, the disturbances from the simulated pile driving in the model with coarse mesh, seemed not to be sufficiently large to induce the complete strain-softening behaviour, shown in figure 5.20. The selected points A, B and C, closest to the pile installation, had some initiation of strain-softening behaviour. Obtaining a distinct peak shear strength and a rapid reduction in shear stresses after the peak was reached. However, the rapid reduction stopped quite suddenly and continued with a very weak reduction of shear stress with increasing strain levels. The points D and E, furthest from the pile installation showed very little of the strain-softening effect, resembling more with the elastic perfectly plastic soil behaviour.

The soil for model with very fine mesh had a quite significant loss of shearing resistance after the peak shear strength was reached. This was due to the choice of relatively low brittleness

ratios to 0.3, which describe a quite brittle soil. The behaviour could be controlled by adjusting the values of the brittleness ratios. Figure 6.1 shows the effect of soil with different brittleness, where the brittleness ratio, (s_{ur}/s_u), described the values of the input parameters $\left(s_{ur}^{A}/{s_u}^{A}\right)$, $\left(s_u^{DSS}{}_r/s_u^A\right)$ and $\left(s_{ur}^{P}/s_u^A\right)$.

The figures show that the curves obtained the same peak shear strength at approximately 19.6 kPa. The post peak response was on the other hand quite dependent of the choice of brittleness. Brittleness ratios from 0.1-0.4 resulted in a strain-softening response leading to slope failure during the simulations, shown in figure 6.1a. Higher choice of brittleness ratios, between 0.5 and 1.0, did however not result in slope failure, shown in figure 6.1b. It may seem that the disturbance was not large enough to provoke the entire strain-softening effect when the brittleness ratios were above 0.4.

Figure 6.1a shows that higher the choice of brittleness ratio, resulted in less reduction of shear stress after attaining the peak and thus a less brittle soil. In this way, it was possible to control the brittleness of the soil by the input parameters that can be obtained from soil testing.

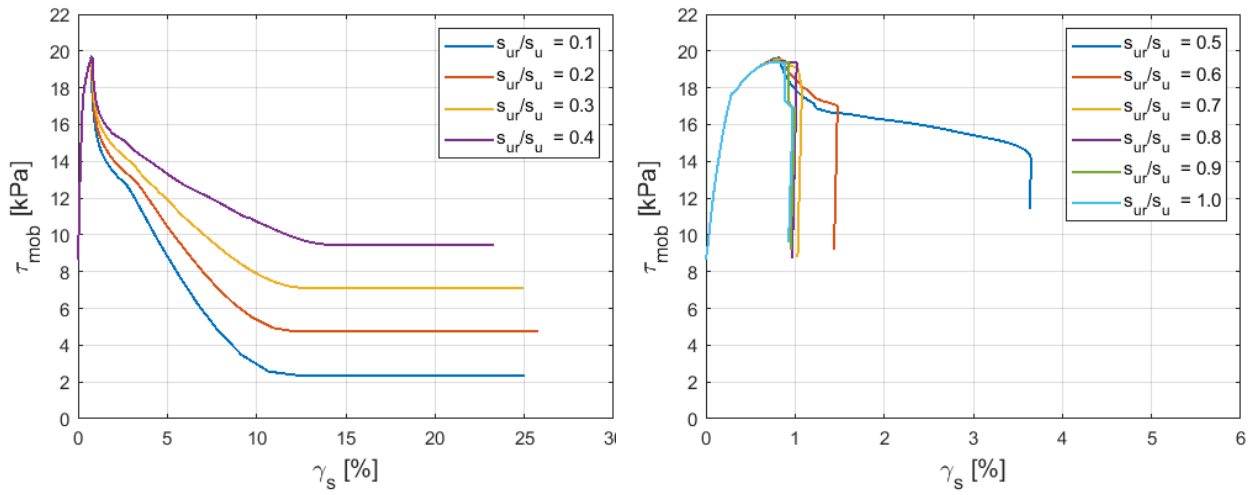

(a) Brittleness ratios between 0.1-0.4.

(b) Brittleness ratios between 0.5-1.0.

Figure 6.1: Shear stress-strain curves plotted with different brittleness ratios.

6.3.2 Progressive failure

The propagation of the failure mechanism was visualised by three steps during the simulations, in figure 5.16. Figure 5.16a shows the onset of the shear strain localisation below the crest of the slope. In figure 5.16b, a shear surface had developed from the pile to the toe of the slope with

strain levels up to 7%. However, the propagation of shear strains seemed to propagate quite simultaneously through the slope. By studying the plots of shear stress versus the steps of the simulation in figure 5.17, it is possible to see that point B reached the peak shear strength some steps before point C, D and E, which reached the peak strength simultaneously.

It seems that there was a more simultaneous mobilisation of shear strength along the critical surface, rather than a progressive one. This response may come from the stepwise manner pile driving was simulated, causing some parts of the soil to be pushed simultaneously. The response from the soil resembled a rigid body movement. A fully progressive failure would require a variable development of deformations along an initiating failure surface. Where there develops zones that experience high levels of straining that cause rapid decrease of shear strength, while other parts of the propagating shear surface has not yet achieved peak shear strength (Bernander, 1978).

It can thus be said that it was possible to see some tendencies of a progressive failure mechanism, based on the fact that point A and B reached a peak shear strength before point C, D and E.

Point A had a somewhat irregular shear strength path, compared to the other points. It seems that the point went in and out of the failure zone during the simulations. By looking at figure 5.16, it is possible to see that the localisation of shear strains shifted positions during the simulations. Probably due to the stepwise installation of the pile, resulting in shear localisation related to the current step expanding. That could explain the irregularities by the point reaching two "peaks" during the simulations.

6.3.3 Shear bands

The failure mechanism in figure 5.13 shows a distinct band where an accumulation of shear strains occurred. This band became nearly 2 m thick, spanning over approximately 7-8 elements. A mechanism that looked quite similar to the occurrence of a shear band, which was defined in the theory section as an area of the soil where deformations develop and accumulates and the soil outside experience elastic unloading (Jostad et al., 2014; Gylland et al., 2014; Thakur, 2011).

As mentioned in section 4.1.3, the NGI-ADPsoft uses a weighting technique to calculate the non-

local strain increments for the material points in the model, replacing the conventional plastic strain increments (Grimstad and Jostad, 2014). The practical implementation in PLAXIS is done by summing up the contributions from material points that is located within a radius of $3l_{int}$ from the material point (Grimstad and Jostad, 2014). Meaning that the plastic strains is averagely distributed to the neighbouring elements controlled by the size of l_{int}. Consequently, the model does not produce a shear band thickness that entirely represents reality, since the model distributes the response to the neighbouring elements and the outcome becomes more spread.

The shear band would presumably be a thin line within the contoured band of shear strains in figure 5.13. The simulations showed that the thickness of the developed band reduced as the internal length was reduced and the mesh size refined accordingly. A finer mesh seemed to give a more accurate result. However, this resulted in much longer calculation time which was troubling in practice.

The intention of the NGI-ADPsoft model was to achieve a response that replicated the stress-strain relationship that is obtained from laboratory testing, such as triaxial tests, for brittle soils. The standard sample sizes in a triaxial test is 10 cm high. The shear stress-strain relationship from a triaxial test is calculated as an average over the entire sample height. In reality, the plastic strains accumulate within the shear band and the soil outside experience next to no plastic deformations. Ideally, the stress-strain response should be calculated by the means of the shear band thickness and not the entire sample height, to capture the realistic behaviour. Hypothetically, this may mean that the strain levels needed to achieve a post-peak softening response may be very large compared the calculated average strain level over the entire sample height. It is however difficult to obtain information about the real stress-strain behaviour inside a shear band. Therefore, an average shear strength-strain distribution is a good approximation.

The shear stress-strain response in figure 5.14 from the model with very fine meshing seemed to sufficiently replicate the response of strain-softening behaviour similar to the response obtained from a brittle soil in a triaxial test. This was however not the case for the model with coarse mesh.

6.3.4 Limitations of the NGI-ADPsoft model

One of the objectives with the simulations with the NGI-ADPsoft model was to obtain a mesh-independent model of slope failure due to the occurrence of strain-softening behaviour. Scaling

the internal length parameter, l_{int}, according to the mesh-size in the areas of expected softening should have given independent results. Materialised by the occurrence of slope failure during the same step of the pile driving simulations. However, the two models with different mesh-size, and internal lengths scaled accordingly did not give the same results. The model with very fine meshing and l_{int} = 0.26 m reached failure at stage 3 of the pile driving simulations. Whereas the model with coarse mesh and l_{int} = 0.96 m, ran through all the pile driving steps without initiating failure. These simulations with the NGI-ADPsoft model did not overcome the problem with dependent results.

Since the NGI-ADPsoft model is a total stress model, the model only generates excess pore pressure due to an increase in total mean stress. Shear-induced excess pore pressure from contractive soil response, is hence not accounted for in the model. The shape of the strain-softening comes from the choice of the softening parameters c_1 and c_2. This means that the strain-softening behaviour in NGI-ADPsoft is seemingly not caused from the generation of shear-induced excess pore pressure diminishing effective stresses, and consequently reducing shear strength. On that account, the distribution of excess pore pressure was not studied for this model.

The model required a significant long calculation time to run through the simulations. Ideally, there should have been tried an analysis with an even smaller internal length parameter, l_{int}, to see the effect on the shear band. According to (Thakur, 2011), the internal length parameter for a soft and sensitive clay may be as low as 0.0002 mm. Internal length parameters with such low values were not possible represent in these analyses.

6.4 Comparison between the Hardening Soil and the NGI-ADPsoft model

The NGI-ADPsoft gave a more realistic representation of the strain-softening response than the HS-model. NGI-ADPsoft gives the possibility of determining the shear strength-strain behaviour to a larger degree. The model is easier to implement for a real soil, since the peak shear strength with corresponding strain level and residual strength with corresponding strain level from soil testing, in fact are the input parameters. In contrary, the strain-softening response in the HS-model was modelled with a negative dilatancy angle and the tension cut-off function in PLAXIS. Which makes it more difficult to determine the stress-strain response from soil test-

ing in terms of the input parameters. The fact that the shear strength-strain response for the NGI-ADPsoft model are directly determinable from soil testing, it makes it more applicable in geotechnical design.

The HS-model was able to account for shear-induced excess pore pressure from contracting behaviour of the soil by implementing negative dilatancy. Whereas the NGI-ADPsoft model did not accounted for this behaviour, since it is a total stress model and can therefore only represent excess pore pressure from a change in the total mean stress situation. By that account, the HS-model managed to represent the pore pressure development more realistically.

Unfortunately, none of the simulations gave entirely independent results. Both constitutive models gave different results depending on mesh-discretisation. The way strain-softening behaviour was modelled in this project could therefore not be implemented in practical engineering. This shows that there is a need for more research on how to implement strain-softening behaviour into geotechnical design.

6.5 Evaluation of the modelling approach

It is not always easy to state which of the effects discussed in this chapter came from the conditions defined in constitutive models and which came from how the boundary conditions and the simulation of pile driving were defined. It seems that the way pile driving was modelled affected how the failure mechanism propagated, triggering the soil to respond in a way that was similar to a rigid body movement. Although pile driving was modelled in a gradual manner, there were still larger sections of the soil being expanding simultaneously. It may be the reason that the soil response was more like a simultaneous mobilisation of shear strength than a progressive one. It may be an idea for the future to study a different approach to model pile driving that would trigger progressive failure more realistically.

Chapter 7

Conclusion

This thesis studied the effect of strain-softening behaviour during pile driving on slope stability. The thesis aimed at answering two research questions. Firstly, to study whether a finite element model could simulate strain-softening of the soil during pile driving. And secondly whether a finite element analysis could model a progressive failure mechanism initiated by the simulated pile driving. This was done by studying the Mohr-Coulomb model, the Hardening Soil model and the NGI-ADPsoft model in PLAXIS.

The Mohr-Coulomb model did not grant the desired effect in terms of reduced stability during the simulated pile driving. Mainly because of the perfectly plastic soil behaviour that did not take contractive behaviour into account. The HS-model with negative dilatancy was able to produce a shear stress-shear strain curve that resembled quite sufficiently the strain-softening behaviour. A failure mechanism was initiated during the analysis. The simulations managed to simulate a progressive failure mechanism to some degree. However, the strain-softening behaviour seemed to developed more simultaneously throughout the failure surface than progressively. These effects were only captured by the model with very fine mesh, as the model with coarse mesh model did not initiate failure during the simulations. Hence, the HS-model with negative dilatancy showed mesh-dependent properties.

Due to the mesh-dependency of the HS-model, the NGI-ADPsoft model was tried. The NGI-ADPsoft model was able to simulate strain-softening behaviour during the modelled pile driving. The strain-softening response was easier to control by the means of the input parameters, since the input could be interpreted directly from soil tests. The model was able to simulate a

failure mechanism of the slope. The failure mechanism showed some tendency towards a progressive failure. However, the way pile driving was modelled seemed to provoke a rigid body behaviour of the soil, that prevented the soil from showing a complete progressive behaviour. Like for the HS-model, the strain-softening behaviour seemed to develop more in a simultaneous manner than progressively.

Although the analyses with the NGI-ADP soft model simulated strain-softening response more sufficiently, it did not overcome the problem with dependent results. The model with very fine mesh and small internal length managed to simulate a failure mechanism, whereas the model with coarse mesh and a larger internal length parameter finished the simulations without initiating failure. These simulations seemed to be mesh-dependent.

7.1 Recommended further work

There are more research and work to be done regarding this subject.

Further study on the NGI-ADPsoft model should be done by means of achieving better understanding of the possibility of obtaining independent results.

Explore further how to achieve a more sufficient simulation of a progressive failure mechanism in the NGI-ADPsoft model. Maybe by changing the way pile driving is modelled.

In long term perspective, research should be done aiming for the development of a method or a set of controls that gives some guidelines on how to take strain-softening and progressive failure directly into account during geotechnical design.

Bibliography

Airhart, T. P., Hirsch, T. J., and Coyle, H. M. (1967). Pile-soil system response in clay as a function of excess pore water pressure and other soil properties. Research Report Number 33-8. Texas Transportation Institute.

Andresen, L. and Jostad, H. (2005). ANISOFT - Constitutive Model for Undrained Loading of Anisotropic and Strain-Softening Clay. *Geo frontiers conference; Soil constitutive models: evaluation, selection, and calibration*, pages 35–44.

Andresen, L. and Jostad, H. P. (2002). A constitutive model for anisotropic and strain-softening clay. *Proc. NUMOG VIII*, pages 79–83. Rome, Italy.

Andresen, L. and Jostad, H. P. (2004). Analyses of progressive failure in long natural slopes. *In Proceedings of the 9th Symposium on Numerical Models in Geomechanics — NUMOG IX*, pages 603–608.

Andresen, L. and Jostad, H. P. (2007). Numerical Modeling of Failure Mechanisms in Sensitive Soft Clay - Application to Offshore Geohazards. *Proceedings of the offshore technology conference*.

Berg-Knutsen, P. (1986). Poreovertrykk i leirige jordarter på grunn av peleramming. Master's thesis, NTH.

Bernander, S. (1978). Brittle failures in normally consolidated soils. *Väg- och vattenbyggaren 8-9*.

Bernander, S., Kullingsjö, A., Gylland, A. S., Bengtsson, P.-E., Knutsson, S., Pusch, R., Olofsson, J., and Elfgren, L. (2016). Downhill progressive landslides in long natural slopes: triggering

agents and landslide phases modeled with a finite difference method. *Canadian Geotechnical Journal*, 53(10):1565.

Bernander, S. and Svensk, I. (1982). On the brittleness of soft clays and its effects on slope stability. *Väg- och Vattenbyggaren*, (7-8).

Bjerrum, L. (1961). The effective Shear Strength Parameters of Sensitive Clays. *Proc. 5th Int. Conf. Soil Mech.*, 1:23–28.

Bjerrum, L. (1968). Progressive failure in slopes of overconsolidated plastic clay and clay shales.

Bjerrum, L. and Johannessen, I. J. (1961). Pore Pressures resulting from driving Piles in Soft Clay. *Norges Geotekniske Institutt*, 41. Oslo.

Bonadies, F., Nordal, S., Gylland, A., Grimstad, G., Jostad, H., Cuomo, S., and Cascini, L. (2014). Numerical methods for simulation of downward progressive landslides. *Numerical Methods in Geotechnical Engineering: Proceedings of the 8th European Conference on Numerical Methods in Geotechnical Engineering*, 1:579–584.

Brinkgreve, R. B. J. (1994). *Geomaterial Models and Numerical Analysis of Softening*. PhD thesis, TU Delft. Delft, The Nederlands.

Duncan, J. M., Wright, S. G., and Brandon, T. L. (2014). *Soil Strength and Slope Stability*. John Wiley & Sons, Inc., Hoboken, New Jersey, 2nd edition.

D'Ignazio, M. and Länsivaara, T. (2015). Shear bands in soft clays: strain-softening behavior in finite element method. *Rakenteiden Mekaniikka*, 48(1):83–98.

Eringen, A. C. (1981). On nonlocoal plasticity. *International Journal of Engineering Science*, 19(12):1461–1474.

Eurocode 7 (2007). Eurocode 7: Geotechnical design - Part 2: Ground investigation and testing. NS-EN1997-2:2007+NA:2008.

Flaate, K. (1971). Effects of pile driving in clays. *Canadian Geotechnical Journal*, 9(1):81–88.

Fornes, P. and Jostad, H. P. (2014). Effekt av progressiv bruddutvikling for utbygging i områder med kvikkleire: Naturfareprosjektet: Delprosjekt 6 kvikkleire. *Norges vassdrags-og energidirektorat*.

Fredriksen, F. (2013). Bysiden. Sig i massene som følge av peleramming.

Fromreide, R. (2019). Evaluation of the effect of pile driving on slope stability. NTNU.

Griffiths, D. V. and Lane, P. A. (1999). Slope stability analysis by finite elements. *Geotechnique*, 49(3):387–403.

Grimstad, G. and Jostad, H. P. (2012). Stability analyses of quick clay using FEM and an anisotropic strain softening model with internal length scale. *Proceedings of the Nordic Geotechnical Meeting*, 2:675—680.

Grimstad, G. and Jostad, H. P. (2014). Effekt av progressiv bruddutvikling for utbygging i områder med kvikkleire: Numerisk metode for beregning av udrenert brudd i sensitive materialer. *Naturfareprosjektet DP.6 Kvikkleire*.

Grimstad, G., Jostad, H. P., and Andresen, L. (2010). Undrained capacity analyses of sensitive clays usinge the non-local strain approach. *9th HSTAM International Congress on Mechanics*, pages 153–160. Limassol, Cyprus.

Grimstad, G., Thakur, V., and Nordal, S. (2005). Experimental Observation on Formation and propagation of shear zone in Norwegian Quick clay. *Landslides and avalanches: 11th ICFL*, pages 137–141. Norway.

Grivas, D. A. and Chowdhury, R. N. (1982). Probabilistic "$\phi = 0°$" stability analysis in strain-softening soil. *Structural Safety*, 1(3):199–210.

Gylland, A., Jostad, H., and Nordal, S. (2014). Experimental study of strain localization in sensitive clays. *Acta Geotechnica*, 9(2):227–240.

Gylland, A. S. (2012). *Material and slope failure in sensitive clays*. PhD thesis, NTNU.

Hoem, O. I. (1975). Endring i poretrykk og stabilitet ved ramming av peler i skråninger. Master's thesis, Norges Tekniske Høgskole.

Huebner, K. H., Dewhirst, D. L., Smith, D. E., and Byrom, T. G. (2001). *The Finite Element Method for Engineers*. Wiley, New York, 4th ed. edition.

Janbu, N. (1973). Slope stability computations. *Embankment Dam Engineering*, pages 47–86. R. C. Hirschfeld and S. J. Poulos eds.

Johansen, S. and Finstad, J. A. (2009). Alarmgrense poretrykksmålere Grønland. Notat RIG 026 - Rev A.

Jostad, H. P. and Andresen, L. (2002). Capacity analysis of anisotropic and strain-softening clays. *Numerical models in geomechanics - NUMOG VIII*.

Jostad, H. P., Andresen, L., and Thakur, V. (2006). Calculation of shear band thickness in sensitive clays. *Proceedings of the 6th numerical methods in geotechnical engineering NUMGE*, pages 27–32. H Schweiger Eds, Graz, Austria.

Jostad, H. P., Fornes, P., and Thakur, V. (2014). *Effect of Strain-Softening in Design of Fills on Gently Inclined Areas with Soft Sensitive Clays*, chapter 24, pages 305–316. Springer Netherlands, Dordrecht.

Jostad, H. P. and Grimstad, G. (2011). Comparison of distribution functions for the non-local strain approach. *2nd International Symposium on Computational Geomecanics (ComGeo II)*. Cavtat-Dubrovnik, Croatia.

Lade, P. V. (2005). Overview of Constitutive Models For Soils. *Soil constitutive models: Evaluation, selection, and calibration*, pages 1–34.

LaGatta, D. P. and Whiteside, S. L. (1984). Failure of a Dredged Slope in a Sensitive Clay. *International Conference on Case Histories in Geotechnical Engineering*.

Langford, J. and Sandene, T. (2015). Effekter av rammede peler i leire - litteraturstudie og erfaringsrapport. *BegrensSkade Delrapport nr. 3.3*.

Locat, A., Leroueil, S., Bernander, S., Demers, D., Jostad, H. P., and Ouehb, L. (2011). Progressive failures in eastern Canadian and Scandinavian sensitive clays. *Canadian Geotechnical Journal*, 48(11):1696–1712.

Massarsch, K. R. and Broms, B. B. (1981). Pile driving in clay slopes. *Proc 10th International Conference on Soil Mechanics and Foundation Engineering*.

Nordal, S. (2019). TBA4116 Geotechnical Engineering, Advanced Course, Lecture notes.

NVE (2014). Sikkerhet mot kvikkleireskred. Vurdering av områdestabilitet ved arealplanleggingog utbygging i områder med kvikkleire og andrejordarter med sprøbruddegenskaper. Veileder nr 7- 2014.

PLAXIS (2018). *PLAXIS 2D Material Models Manual 2018*.

PLAXIS (2019). *PLAXIS 2D Reference Manual 2019*.

Prévost, J. H. and Höeg, K. (1975). Soil mechanics and plasticity analysis of strain softening. *Géotechnique*, 25(2):279–297.

Rosenqvist, I. T. (1953). Considerations on the Sensitivity of Norwegian Quick-Clays. *Géotechnique*, 3(5):195–200.

Schanz, T., Vermeer, P. A., and Bonnier, P. G. (2000). The hardening soil model: Formulation and verification. *Proceedings Plaxis Symposium "Beyond 2000 in Computational Geotechnics"*, pages 281–296. Balkema, Amsterdam, The Netherlands.

Skempton, A. W. (1964). Long-Term Stability of Clay Slopes. *Géotechnique*, 14(2):77–102.

Statens Vegvesen (2005). Laboratorieundersøkelser. *Håndbok 014*. Vedlegg 1.

Thakur, V. (2007). *Strain Localizations in Sensitive Soft Clays*. PhD thesis, NTNU.

Thakur, V. (2011). Numerically observed shear bands in soft sensitive clays. *Geomechanics and Geoengineering*, 6(2):131–146.

Thakur, V., Grimstad, G., and S.Nordal (2006). Instability in Soft Sensitive Clays. ECI: Geohazards and Risk Evaluation conference. Farrokh Nadim, Rudolf Pöttler, Herbert Einstein, Herbert Klapperich, and Steven Kramer Eds, ECI Symposium Series, Norway. Vol. P7. http://services.bepress.com/eci/geohazards/43.

Thakur, V., Jostad, H. P., Kornbrekke, H. A., and Degago, S. A. (2014). *How Well Do We Understand the Undrained Strain Softening Response in Soft Sensitive Clays?*, chapter 23, pages 291–303. Springer Netherlands, Dordrecht.

Thakur, V., Nordal, S., Jostad H, P., and Andresen, L. (2005). Study on pore water pressure dissipation during shear banding in sensitive clays. *11th International conference on computer methods and advances in geomechanics*, 4:289–296. G Barla and M Barla Eds, Italy.

Yu, H. S., Salagdo, R., Sloan, W., and Kim, J. M. (1998). Limit Analysis versus Limit Equilibrium for Slope Stability. *Journal of Geotechnical and Geoenvironmental Engineering*, 124(1):1–11.